



Finite element methods for time-dependent convection–diffusion–reaction equations with small diffusion

Volker John*, Ellen Schmeier¹

FR 6.1 – Mathematik, Universität des Saarlandes, Postfach 15 11 50, 66041 Saarbrücken, Germany

ARTICLE INFO

Article history:

Received 14 May 2008

Received in revised form 25 August 2008

Accepted 28 August 2008

Available online 12 September 2008

Keywords:

Time-dependent convection–diffusion–reaction equations
Finite element methods
Small diffusion parameter
Spurious oscillations

ABSTRACT

Numerical studies of stabilized finite element methods for solving scalar time-dependent convection–diffusion–reaction equations with small diffusion are presented in this paper. These studies include the streamline-upwind Petrov–Galerkin (SUPG) method with different parameters, various spurious oscillations at layers diminishing (SOLD) methods, a local projection stabilization (LPS) scheme based on enrichment and two finite element method flux corrected transport (FEM-FCT) methods. The focus of the evaluation of the numerical results is on the reduction of spurious oscillations.

© 2008 Elsevier B.V. All rights reserved.

1. Introduction

The simulation of time-dependent convection–diffusion–reaction equations is required in various applications. A typical example is the simulation of processes which involve a chemical reaction in a flow field. Such reactions are modeled by a non-linear system of time-dependent convection–diffusion–reaction equations for the concentrations of the reactants and the products. These equations are strongly coupled such that inaccuracies in one concentration directly affect all other concentrations. Typically, the size of the diffusion is smaller by several orders of magnitude compared to the size of the flow field. That means, the convection–diffusion–reaction equations are convection-dominated. Often, there is also a strong chemical reaction such that the equations become reaction-dominated, too. A characteristic feature of solutions of convection- and reaction-dominated equations is the presence of sharp layers. The accurate simulation of such processes requires numerical methods which are, on the one hand, able to compute sharp layers and which prevent, on the other hand, the occurrence of spurious oscillations.

A special example of processes with chemical reactions in a flow field are precipitation processes. In [39], a calcium carbonate precipitation was simulated, where the system of time-dependent

convection–diffusion–reaction equations was discretized in time with the Crank–Nicolson scheme and in space with the Q_1 finite element method. Since the equations in the system are convection- and reaction-dominated, a stabilization of the finite element discretization is necessary. In [39], the standard streamline-upwind Petrov–Galerkin (SUPG) method [30,7] with the parameter from [49] was used. This approach led to computed concentrations with considerable spurious oscillations, see Fig. 1 for an illustration. In the simulations presented in [39], which use laminar flow fields in 2D, negative oscillations (negative concentrations) were just cut off. We could observe in further numerical tests that increasing the Reynolds number of the flow fields in 2D or performing simulations in 3D (on coarser grids) led to a piling up of the remaining positive oscillations and finally to a blow-up of the simulations. Likewise, in [39] is reported that the use of a very diffusive upwind scheme led to unphysical results. Hence, there is the need of better methods, namely methods which fulfill the two requirements given above.

The first step in identifying appropriate methods for the accurate simulation of the chemical reaction process is of course the consideration of scalar time-dependent convection–diffusion–reaction equations. The code which is used for the simulation of the precipitation process is based on finite element methods. We will concentrate in this paper on first order finite elements, which are the simplest and most often used finite elements.

A study of stabilized finite element methods for time-dependent convection–diffusion–reaction equations can be found in [14]. This study clarified similarities and differences between several methods, among them the SUPG method. The basic idea in the

* Corresponding author. Tel.: +49 681 302 4445; fax: +49 681 302 3046.

E-mail addresses: john@math.uni-sb.de (V. John), schmeier@math.uni-sb.de (E. Schmeier).

¹ The research of E. Schmeier was supported by the Deutsche Forschungsgemeinschaft (DFG) by Grant No. Jo 329/8-1.

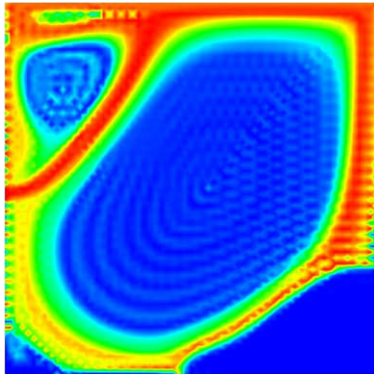


Fig. 1. Spurious oscillations of a concentration in the simulation of a precipitation process computed with the SUPG method.

application of stabilized finite element methods is that after the temporal discretization of the time-dependent equation, the equation has the form of a steady-state convection–diffusion–reaction equation. Appropriate parameters for the SUPG method applied to steady-state convection–diffusion–reaction equations have been studied in [15] and for the unusual stabilized finite element method (USFEM) in [20]. Steady-state convection–diffusion–reaction equations with positive and negative reactive terms (source terms) were considered in [26]. A non-linear extension of the SUPG approach which tries to reduce spurious oscillations, which is similar to the SOLD method KLR02 in the present paper, was analyzed in [42]. The analysis was extended to higher order finite elements, taking the polynomial degree into account, in [49]. Finite element methods for time-dependent convection–diffusion–reaction equations which are based on variational multiscale principles were considered e.g. in [16,27,33,24].

Since it has been known for a long time that the SUPG method leads to solutions with spurious oscillations also for steady-state convection–diffusion equations, several methods have been proposed to reduce or to remove these oscillations. These methods are called Spurious Oscillations at Layers Diminishing (SOLD) methods, see [34,36] for a review. However, very few of them have been so far used in the simulation of time-dependent equations, see [2] for an example.

In recent years, local projection stabilization (LPS) schemes have been developed for stabilizing convection-dominated problems [3,5,6]. A scheme of this type was used for the computation of steady-state convection–diffusion equations in [50]. We are not aware that LPS schemes were applied already in the simulation of time-dependent convection–diffusion–reaction equations.

All approaches mentioned so far try to stabilize the finite element method by adding additional terms to the Galerkin finite element discretization. A different approach are finite element method flux corrected transport (FEM-FCT) schemes [46,45,44,43]. These schemes work on the algebraic level, that means they modify the algebraic equation which is obtained from the Galerkin finite element method. Roughly speaking, this equation is firstly replaced with an equation representing a low order scheme which introduces too much diffusion. Then, the diffusion is removed again in regions where it is not needed by modifying the right hand side. The modifications are based on an auxiliary solution which is computed with a non-oscillatory explicit scheme.

This paper presents first steps in identifying appropriate finite element methods for the simulation of scalar time-dependent convection–diffusion–reaction equations. Many of the available methods, like SUPG methods with different parameters, various SOLD methods, a LPS scheme and two FEM-FCT methods are compared numerically. To our best knowledge, many of these methods have

not yet been used in the simulation of time-dependent problems so far. In addition, it seems to be the first comparison of FEM-FCT methods to more traditional schemes for the stabilization of finite element methods of convection-dominated and reaction-dominated equations. The main goal of the paper consists in identifying those methods which show the capability to improve the solution obtained with the SUPG method considerably.

The paper is organized as follows. Section 2 presents the equations, the temporal discretization and introduces notations. In Section 3, the SUPG method is described and available proposals for the parameter are reviewed. Section 4 is devoted to the description of the SOLD methods. The LPS scheme will be introduced in Section 5 and the FEM-FCT schemes in Section 6. Section 7 contains the numerical studies and the evaluation of the methods. The conclusions are summarized in Section 8.

2. Basic discretizations

Throughout the paper, we use the standard notations $L^p(\Omega)$ for Lebesgue spaces and $W^{k,p}(\Omega)$, $H^k(\Omega) = W^{k,2}(\Omega)$ for Sobolev spaces. The inner product in the space $L^2(\Omega)$ will be denoted by (\cdot, \cdot) . For a vector $\mathbf{b} \in \mathbb{R}^d$, the symbol $\|\mathbf{b}\|_2$ stands for its Euclidean norm.

We consider the scalar convection–diffusion–reaction equation

$$u_t - \varepsilon \Delta u + \mathbf{b} \cdot \nabla u + cu = f \quad \text{in } (0, T] \times \Omega, \quad (1)$$

where $\varepsilon > 0$ is the diffusion coefficient, $\mathbf{b} \in L^\infty(0, T; W^{1,\infty}(\Omega))^d$ is the convection field with $\nabla \cdot \mathbf{b} = 0$, $c \in L^\infty(0, T; L^\infty(\Omega))$ is the non-negative reaction coefficient, $f \in L^2(0, T; L^2(\Omega))$, $T > 0$ is the final time and $\Omega \subset \mathbb{R}^d$, $d \in \{2, 3\}$, is a bounded domain. This equation has to be equipped with appropriate boundary conditions and an initial condition $u_0 = u(0, \mathbf{x})$.

We will consider fractional-step θ -schemes as temporal discretization of (1). These schemes applied to (1) lead at the discrete time t_k to an equation of the form

$$\begin{aligned} u_k + \theta_1 \Delta t_k (-\varepsilon \Delta u_k + \mathbf{b} \cdot \nabla u_k + cu_k) \\ = u_{k-1} - \theta_2 \Delta t_k (-\varepsilon \Delta u_{k-1} + \mathbf{b} \cdot \nabla u_{k-1} + cu_{k-1}) \\ + \theta_3 \Delta t_k f_{k-1} + \theta_4 \Delta t_k f_k \end{aligned} \quad (2)$$

with $\Delta t_k = t_k - t_{k-1}$ and the parameters $\theta_1, \dots, \theta_4$. The backward Euler scheme is obtained for $\theta_1 = \theta_4 = 1$, $\theta_2 = \theta_3 = 0$ and the Crank–Nicolson scheme for $\theta_1 = \theta_2 = \theta_3 = \theta_4 = 0.5$. Eq. (2) can be considered as a stationary convection–diffusion–reaction equation at t_k with the diffusion, convection and reaction, respectively, given by

$$D = \theta_1 \Delta t_k \varepsilon, \quad (3)$$

$$\mathbf{C} = \theta_1 \Delta t_k \mathbf{b}, \quad (4)$$

$$R = 1 + \theta_1 \Delta t_k c. \quad (5)$$

Eq. (2) will be discretized with a finite element method. To apply such a method, (2) can be transformed into a weak formulation in the usual way by multiplying with test functions from an appropriate space V and applying integration by parts. Finite element methods employ now a finite dimensional space V^h instead of V . For simplicity of presentation, homogeneous Dirichlet conditions and conforming finite elements, $V^h \subset V$, are considered. A Galerkin finite element problem arising from (2) reads as follows: Find $u_k^h \in V^h$ such that

$$\begin{aligned} (u_k^h, {}^h) + \theta_1 \Delta t_k ((\varepsilon \nabla u_k^h, \nabla^h) + (\mathbf{b} \cdot \nabla u_k^h + cu_k^h, {}^h)) \\ = (u_{k-1}^h, {}^h) - \theta_2 \Delta t_k ((\varepsilon \nabla u_{k-1}^h, \nabla^h) + (\mathbf{b} \cdot \nabla u_{k-1}^h + cu_{k-1}^h, {}^h)) \\ + \theta_3 \Delta t_k (f_{k-1}, {}^h) + \theta_4 \Delta t_k (f_k, {}^h) \end{aligned} \quad (6)$$

for all ${}^h \in V^h$. The definition of V^h is usually based on an underlying triangulation \mathcal{T}^h of Ω . We assume that this triangulation fulfills the usual compatibility conditions, see [12].

It is well known that in the case of dominant convection or reaction, the Galerkin finite element formulation becomes unstable and the solution of (6) shows spurious oscillations in the whole domain.

3. The SUPG method

3.1. The general approach

A popular finite element stabilization method for convection-dominated problems is the streamline-upwind Petrov–Galerkin (SUPG) method [30,7], which adds a consistent diffusion term in streamline direction

$$\sum_{K \in \mathcal{T}^h} \tau_K (\text{residual of (2), } \mathbf{C} \cdot \nabla v^h)_K \quad (7)$$

to (6), where $\{\tau_K\}$ is a set of parameters depending on the mesh cells $K \in \mathcal{T}^h$, $(\cdot, \cdot)_K$ is the inner product in $L^2(K)$ and \mathbf{C} denotes the convection. The residual is defined by the difference of the left hand side and the right hand side of (2).

Inserting (7) into (6), using the convection given by (4) and rearranging terms lead to

$$\begin{aligned} & (u_k^h, v^h) + \sum_{K \in \mathcal{T}^h} (\tau_K \theta_1 \Delta t_k) (u_k, \mathbf{b} \cdot \nabla v^h)_K \\ & + \theta_1 \Delta t_k \left[(\varepsilon \nabla u_k^h, \nabla v^h) + (\mathbf{b} \cdot \nabla u_k^h + cu_k^h, v^h) \right. \\ & \left. + \sum_{K \in \mathcal{T}^h} (\tau_K \theta_1 \Delta t_k) ((-\varepsilon \Delta u_k + \mathbf{b} \cdot \nabla u_k + cu_k), \mathbf{b} \cdot \nabla v^h)_K \right] \\ & = (u_{k-1}^h, v^h) + \sum_{K \in \mathcal{T}^h} (\tau_K \theta_1 \Delta t_k) (u_{k-1}, \mathbf{b} \cdot \nabla v^h)_K \\ & - \theta_2 \Delta t_k \left[(\varepsilon \nabla u_{k-1}^h, \nabla v^h) + (\mathbf{b} \cdot \nabla u_{k-1}^h + cu_{k-1}^h, v^h) \right. \\ & \left. + \sum_{K \in \mathcal{T}^h} (\tau_K \theta_1 \Delta t_k) ((-\varepsilon \Delta u_{k-1} + \mathbf{b} \cdot \nabla u_{k-1} + cu_{k-1}), \mathbf{b} \cdot \nabla v^h)_K \right] \\ & + \theta_3 \Delta t_k \left[(f_{k-1}, v^h) + \sum_{K \in \mathcal{T}^h} (\tau_K \theta_1 \Delta t_k) (\Delta t_k f_{k-1}, \mathbf{b} \cdot \nabla v^h)_K \right] \\ & + \theta_4 \Delta t_k \left[(f_k, v^h) + \sum_{K \in \mathcal{T}^h} (\tau_K \theta_1 \Delta t_k) (\Delta t_k f_k, \mathbf{b} \cdot \nabla v^h)_K \right]. \quad (8) \end{aligned}$$

3.2. Proposals for the parameter

The crucial question in the application of the SUPG stabilization is of course the choice of the parameters $\{\tau_K\}$. There is a large amount of literature concerning this choice in the case that the reaction term is absent. However, for the time-dependent convection–diffusion–reaction equations, the reaction (5) might dominate the diffusion (3) and the convection (4), in particular for small time steps. Thus, appropriate parameters should take the reaction into account, see also the numerical studies in Example 7.1. There are several proposals in the literature for such parameters. Let D, \mathbf{C}, R be the abbreviations for diffusion, convection and reaction, respectively, where we are interested in particular in the expressions given in (3)–(5).

In [15], it was proposed to set the parameter on the mesh cell K to be

$$\tau_K^{\text{Cod}} \sim \left(\frac{4|D|}{h_K^2} + \frac{2\|\mathbf{b}\|_2}{h_K} + |R| \right)^{-1}$$

which gives for (3)–(5)

$$\tau_K^{\text{Cod}} \sim \frac{h_K^2}{4\theta_1 \Delta t_k \varepsilon + 2h_K \theta_1 \Delta t_k \|\mathbf{b}\|_2 + h_K^2 (1 + \theta_1 \Delta t_k c)}. \quad (9)$$

Here, h_K is an appropriate measure for the size of the mesh cell K . Note that τ_K depends in general on the point $\mathbf{x} \in K$.

In [20], the parameter

$$\tau_K^{\text{FV}} \sim \frac{h_K^2}{|R|h_K^2 \xi(Pe_{K,1}) + (2|D|/m_K)\xi(Pe_{K,2})}$$

with

$$Pe_{K,1} = \frac{2|D|}{m_K |R| h_K^2}, \quad Pe_{K,2} = \frac{m_K \|\mathbf{C}\|_2 h_K}{|D|}, \quad \xi(\kappa) = \begin{cases} 1 & 0 \leq \kappa \leq 1, \\ \kappa & \kappa \geq 1 \end{cases}$$

was proposed for the unusual finite element method (USFEM). This parameter was used in the SUPG method in [26]. The parameter m_K comes from an inverse estimate. For linear finite elements, it is $m_K = 1/3$, which holds in practice also for bilinear finite elements [26]. Inserting (3)–(5) gives

$$\tau_K^{\text{FV}} \sim \frac{h_K^2}{(1 + \theta_1 \Delta t_k c) h_K^2 \xi(Pe_{K,1}) + 6\theta_1 \Delta t_k \varepsilon \xi(Pe_{K,2})} \quad (10)$$

with

$$Pe_{K,1} = \frac{6\theta_1 \Delta t_k \varepsilon}{h_K^2 (1 + \theta_1 \Delta t_k c)}, \quad Pe_{K,2} = \frac{h_K \theta_1 \Delta t_k \|\mathbf{b}\|_2}{3\theta_1 \Delta t_k \varepsilon} = \frac{h_K \|\mathbf{b}\|_2}{3\varepsilon}.$$

The appropriate measure of the mesh cell h_K is also discussed in [20]. It is proposed to set h_K as the diameter of the mesh cell in the direction of the convection, see also [34] for a discussion of this topic.

In [42,49], it is proposed to set

$$\tau_K^{\text{KLR}} \sim \min \left\{ \frac{h_K}{p_K \|\mathbf{C}\|_{L^\infty(K)}}, \frac{1}{\|\mathbf{R}\|_{L^\infty(K)}}, \frac{h_K^2}{p_K^4 c_{\text{inv}}^2 \|D\|_{L^\infty(K)}} \right\},$$

where p_K is the polynomial degree of the finite element in the mesh cell K and c_{inv} is a constant from an inverse estimate. We consider (bi-)linear finite elements, i.e. $p_K = 1$ and $c_{\text{inv}} = 1$. From the computational point of view, it is easier to replace the norms in $L^\infty(K)$ by the norms which are used in the other proposals of the stabilization parameter. Thus, we consider

$$\tau_K^{\text{KLR}} \sim \min \left\{ \frac{h_K}{2\|\mathbf{C}\|_2}, \frac{1}{|R|}, \frac{h_K^2}{|D|} \right\},$$

where also the factor $1/2$ was introduced in the first term, see the discussion below of some limit cases for the different parameters. Inserting (3)–(5) leads to

$$\tau_K^{\text{KLR}} \sim \min \left\{ \frac{h_K}{2\theta_1 \Delta t_k \|\mathbf{b}\|_2}, \frac{1}{1 + \theta_1 \Delta t_k c}, \frac{h_K^2}{\theta_1 \Delta t_k \varepsilon} \right\}. \quad (11)$$

It turns out that all three proposals of the parameters give similar results in some interesting limit cases. Consider first the convection-dominated regime, where the local Péclet number is large

$$Pe_K = \frac{\|\mathbf{b}\|_2 h_K}{2\varepsilon} \gg 1$$

with $\|\mathbf{b}\|_2 = \mathcal{O}(1)$ from which follows $\varepsilon \ll h_K$. If $\Delta t_k \ll h_K \ll 1$, then one obtains

$$\tau_K^{\text{Cod}} \sim \tau_K^{\text{FV}} \sim \tau_K^{\text{KLR}} \sim \frac{1}{1 + \theta_1 \Delta t_k c},$$

where $Pe_{K,1} < 1$ in the definition of τ_K^{FV} . This case is of interest if fast reactive processes are modeled, whose numerical simulation requires the use of a small time scale. Another case which might occur often in applications is $\Delta t_k \sim h_K \ll 1$. This gives

$$\tau_K^{Cod} \sim \tau_K^{FV} \sim \frac{h_K}{2\theta_1 \Delta t_k \|\mathbf{b}\|_2 + h_K(1 + \theta_1 \Delta t_k c)},$$

$$\tau_K^{KLR} \sim \min \left\{ \frac{h_K}{2\theta_1 \Delta t_k \|\mathbf{b}\|_2}, \frac{1}{1 + \theta_1 \Delta t_k c} \right\}.$$

Clearly, if \sim is replaced by $=$, then $\tau_K^{KLR} \geq \tau_K^{Cod}, \tau_K^{FV}$ in this case. The ratio $\tau_K^{KLR}/\tau_K^{Cod}$ depends on all inputs in the definition of the parameters. Fig. 2 shows that τ_K^{KLR} might be considerably larger than the other parameters. Very similar pictures as in this figure are obtained for $c = 0$.

In applications like in [39], the convection field \mathbf{b} is often a velocity field which was computed by solving the Navier–Stokes equations numerically. This velocity field might have regions where $\|\mathbf{b}\|_2$ is small and generally c is small in these regions, too. Considering the limit $\|\mathbf{b}\|_2 \rightarrow 0, c = 0$, one obtains for the parameters, in the case $h_K^2 \gg \Delta t_k \varepsilon$,

$$\tau_K^{Cod} \sim \tau_K^{FV} \sim \tau_K^{KLR} \rightarrow 1,$$

see also Fig. 3. Since the SUPG term vanishes for $\|\mathbf{b}\|_2 \rightarrow 0$, thus it vanishes in the same way for all stabilization parameters.

Remark. The appropriate measure of the mesh cell h_K should be chosen as the length of the mesh cell in the direction of the convection for scalar convection–diffusion equations [53,20,34]. This choice is recommended also in the case of steady-state convection–diffusion–reaction equations in [20]. However, it is not clear if this remains the appropriate choice if the reaction dominates convection very strongly as in the case of time-dependent equations with small time steps. The contribution of the reaction R will dominate all parameters in this case. This term does not involve the mesh size and thus the actual choice of h_K is of minor importance. In fact, numerical studies (not presented here) showed that one obtains almost identical results as presented in Section 7 if h_K is simply chosen to be the diameter of the mesh cell K .

Remark. The stability of the SUPG method applied to time-dependent convection–diffusion equations was studied analytically in [4]. It was proven that the coupling of the SUPG method to implicit time stepping schemes leads to a stable discretization, regardless of the length of the time step. In addition, it is pointed out that spurious oscillations may be expected for small time steps, which can be observed also in the numerical studies presented in [4] and in Section 7.

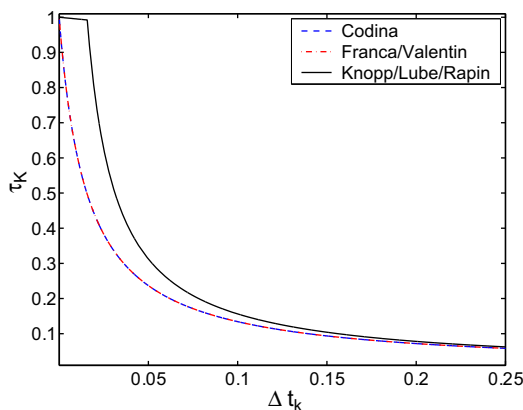


Fig. 2. SUPG parameters $\tau_K^{Cod}, \tau_K^{FV}, \tau_K^{KLR}$ for $\varepsilon = 10^{-6}, \|\mathbf{b}\|_2 = 1, c = 1, \theta_1 = 0.5$ and $h_K = 1/64$. The curves of τ_K^{Cod} , and τ_K^{FV} are on top of each other. Right picture: ratio of τ_K^{KLR} and τ_K^{Cod} .

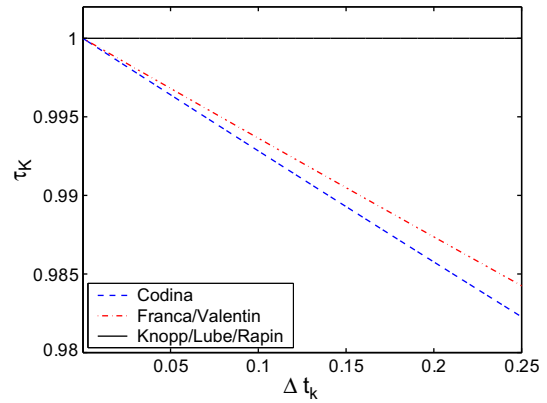


Fig. 3. SUPG parameters $\tau_K^{Cod}, \tau_K^{FV}, \tau_K^{KLR}$ for $\varepsilon = 10^{-6}, \|\mathbf{b}\|_2 = 10^{-3}, c = 0, \theta_1 = 0.5$ and $h_K = 1/64$.

4. SOLD methods

SOLD methods have been developed to reduce or even to remove spurious oscillations at layers from SUPG finite element solutions of steady-state scalar convection–diffusion equations. One can distinguish several classes of SOLD methods, see the reviews [34,36]. These reviews reveal that currently there is no SOLD method which generally works satisfactorily. Some of the SOLD methods improve the results of the SUPG discretization considerably in special examples. But in [34–36], for each SOLD method examples were found where it fails.

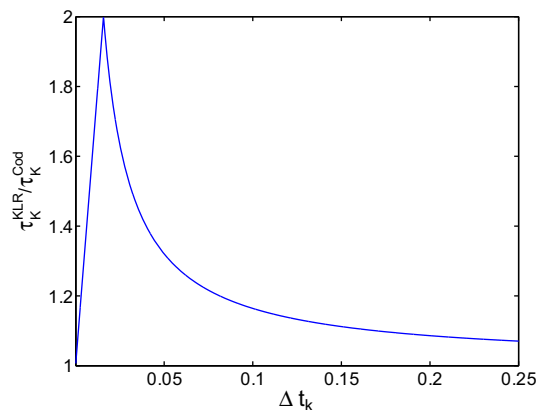
Most of the SOLD methods were derived for equations with convection and diffusion but without reactive term. There are only few examples in which SOLD methods were used for the simulation of time-dependent problems [2].

In the numerical studies presented in Section 7, a number of SOLD methods which have been studied for steady-state equations in [34–36] will be used in the simulation of time-dependent convection–diffusion–reaction equations. These studies should give first impressions on the effect of the SOLD methods in equations of this kind and they should provide hints for improving the methods.

The numerical studies in Section 7 investigate SOLD methods which add isotropic diffusion

$$(\tilde{\varepsilon} \nabla u_k^h, \nabla v^h), \tag{12}$$

SOLD methods which add anisotropic diffusion (orthogonal to the streamlines)



$$(\tilde{\epsilon} C_{os} \nabla u_k^h, \nabla v^h), \tag{13}$$

where

$$C_{os} = \begin{cases} I - \frac{C \cdot C}{\|C\|_2^2} & \text{if } C \neq 0, \\ 0 & \text{else,} \end{cases}$$

and edge stabilization methods. Obviously, the convection C from (4) in the definition of C_{os} can be replaced by b .

The terms (12) and (13) appear only on the left hand side of (8). In the following, all parameters have to be understood in the way that they are replaced by zero if the denominator of the formula vanishes.

4.1. Isotropic SOLD methods

The parameter of most of the investigated methods for the isotropic SOLD stabilization (12) has the general form

$$\tilde{\epsilon} = \sigma \frac{|R^h(u_k^h)|^2}{\|\nabla u_k^h\|_2^2}, \tag{14}$$

where $R^h(u_k^h)$ is the residual of (2) (right hand side subtracted from left hand side).

The definition of the parameter σ for many isotropic SOLD stabilizations of steady-state convection–diffusion equations is motivated with the help of an appropriate streamline direction such that the discrete solution fulfills on each mesh cell the strong form of the equation, see [34]. Minimizing the Euclidean norm of the difference of all possible appropriate streamline directions and the convection gives an auxiliary vector z^h . It is much harder to determine appropriate streamline directions for (2) based on the same motivation. Therefore, we use in the simulations presented in this paper in principle the same auxiliary vector as it is proposed for steady-state convection–diffusion problems. Since this vector is obtained with a minimization to the convection, it becomes clear that this vector has to be scaled appropriately for time-dependent problems, leading to

$$z^h = \theta_1 \Delta t_k \frac{R^h(u^h) \nabla u^h}{\|\nabla u^h\|_2^2}.$$

The first scheme which will be considered was proposed in [22] (GdC88) where

$$\sigma|_K = \max\{0, \tau_K(z^h) - \tau_K\}. \tag{15}$$

Here, τ_K is the chosen SUPG stabilization parameter and $\tau_K(z^h)$ is this SUPG parameter evaluated for the convection z^h instead of C . For the diffusion and reaction, we used the values D and R from (3) and (5), respectively. For small time steps, the definition of $\tau_K(z^h)$ and τ_K will be dominated both by the reactive term R , leading to (almost) the same values. Thus, it can be expected that σ is in general small and the results of GdC88 differ not much from the results obtained with the SUPG method. This expectation will be confirmed in the numerical studies. The parameter of GdC88 is influenced by the time step Δt_k only indirectly over the residual in z^h and over the SUPG parameter.

The proposal of [19] (dCG91) has the form

$$\sigma|_K = \tau_K \left\{ 0, \frac{\|C\|_2}{\|z^h\|_2} - 1 \right\}.$$

This formula also suggests that z^h should be scaled the same way with respect to Δt_k as C .

In [1] (AS97), the parameter

$$\sigma|_K = \tau_K \left\{ 0, \frac{\|C\|_2}{\|z^h\|_2} - \xi^h \right\}, \quad \xi^h = \max \left\{ 1, \frac{C \cdot \nabla u^h}{R^h(u^h)} \right\}$$

was proposed. In this method, a small time step will generally lead to $\xi^h = 1$ such that a similar behavior of the simulations like for the SOLD method dCG91 can be expected.

Another isotropic SOLD method with the parameter $\tilde{\epsilon}$ of form (14) was suggested in [18] (dCA03). The parameter of dCA03 is an extended version of GdC88 where (15) is multiplied with an appropriate factor. The definition of this factor is rather involved, see [34] for details. For the same reasons as for GdC88, it can be expected that the results of dCA03 will not differ much from the SUPG results.

In [54], the so-called YZ β shock capturing scheme was proposed for the simulation of compressible flows. This scheme was transferred to time-dependent convection–diffusion equations in [2] and applied to the simulation of an arterial drug delivery problem. In [2], the YZ β parameter was used in an isotropic diffusion term of form (12). This parameter has the form

$$\tilde{\epsilon} = |Y|^{-\beta+1} |R^h(u^h)| \|\nabla u^h\|_2^{\beta-2} \left(\frac{\tilde{h}_K}{2} \right)^\beta,$$

where Y is a global reference value for the solution, $\beta \in \{1, 2\}$ and \tilde{h}_K is the diameter of the mesh cell in direction of ∇u^h . This size can be easily approximated, see [55,34]. In [2], some numerical tests suggest that the choice $\beta = 1$ leads to better results than $\beta = 2$. For this reason, we will restrict our numerical studies to the case $\beta = 1$, which leads to the parameter

$$\tilde{\epsilon} = \frac{\tilde{h}_K |R^h(u^h)|}{2 \|\nabla u^h\|_2}. \tag{16}$$

This parameter will be influenced by the length of the time step only over the residual.

4.2. Anisotropic SOLD methods

An anisotropic SOLD method which will be studied was proposed in [13] (C93)

$$\tilde{\epsilon}|_K = \max \left\{ 0, C \frac{\text{diam}(K) |R^h(u_k^h)|}{2 \|\nabla u_k^h\|_2} - D \frac{|R^h(u_k^h)|}{\|C\|_2 \|\nabla u_k^h\|_2} \right\}, \tag{17}$$

where C is a user-chosen constant (or parameter), $\text{diam}(K)$ is the diameter of the mesh cell K , i.e. the longest distance of two points of the closure of K , and

$$C^l = \frac{(C \cdot \nabla u_k^h) \nabla u_k^h}{\|\nabla u_k^h\|_2^2}.$$

The length of the time step has no direct influence on the parameters of C93.

A similar form of the parameter was considered in [42,34] (KLR02)

$$\tilde{\epsilon}|_K = \max \left\{ 0, C \frac{\text{diam}(K) |R^h(u_k^h)|}{2 \|\nabla u_k^h\|_2} - D \right\}. \tag{18}$$

The second term of (17) and (18) will be small for small diffusions D . However, the definition of the second term in (17) introduces another non-linearity into the scheme compared to (18). The numerical studies in Section 7 will reveal that this additional non-linearity has a negative effect on the efficiency of the iterative scheme for solving the non-linear problems.

In [8,34] (BE02_2), the parameter

$$\tilde{\epsilon} = \frac{\tau \|C\|_2^2 |R^h(u_k^h)|}{\|C\|_2 \|\nabla u_k^h\|_2 + |R^h(u_k^h)|} \tag{19}$$

was proposed. This is a simplification of a parameter derived in [9,8] (BE02_1). To obtain the parameter of BE02_1, (19) is multiplied by a

longer factor. This factor tends to 1 for small time steps such that similar results can be expected for BE02_1 and BE02_2. The parameters of BE02_1 and BE02_2 scale quadratically with the length of the time step. For these two methods, only a small effect of the SOLD term can be expected for small time steps, see Section 7.

Since there is no motivation in [2] for using the $YZ\beta$ parameter (16) in the isotropic diffusion (12), we will study this parameter also for the anisotropic diffusion (13). Note, this parameter is similar to the first parts of the parameters of C93 (17) and KLR02 (18). Apart from the scaling factor C , only the used measure for the size of the mesh cell differs. This seems to be a slight change, however in contrast to $\text{diam}(K)$, the mesh cell measure h_K is non-linear. This might affect the efficiency of the iterative scheme for solving the non-linear problems negatively.

The only linear SOLD method which will be considered in the numerical studies was proposed in [41] (JSW87). It adds anisotropic diffusion (13) and has the parameter

$$\tilde{\varepsilon}|_K = \max\{0, \|\mathbf{C}\|_2 h_K^{3/2} - D\} \quad \forall K \in \mathcal{T}^h. \quad (20)$$

The parameter of JSW87 scales linearly with Δt_k . In our numerical studies, we could observe that the unscaled version of JSW87, i.e., with the parameter

$$\tilde{\varepsilon}|_K = \max\{0, \|\mathbf{b}\|_2 h_K^{3/2} - \varepsilon\} \quad \forall K \in \mathcal{T}^h$$

is by far too diffusive. Already after a short simulation time, all layers were smeared extensively.

4.3. Edge stabilization methods

Edge stabilization methods add a term of the form

$$\sum_{K \in \mathcal{T}^h} |K| \int_{\partial K} \Psi_K(u_K^h) \text{sign} \left(\frac{\partial u_K^h}{\partial \mathbf{t}_{\partial K}} \right) \frac{\partial v^h}{\partial \mathbf{t}_{\partial K}} d\sigma,$$

where ∂K is the boundary of the mesh cell K , $|K|$ is its measure, $\mathbf{t}_{\partial K}$ a tangential vector on the faces of the boundary and sign denotes the signum function. The appearance of the factor $|K|$ is motivated in [36].

There are several proposals for the parameter function $\Psi_K(u_K^h)$. One goes back to [11] (BH04)

$$\Psi_K(u_K^h) = \frac{\text{diam}(K)}{|K|} (C_0 D + C_1 \text{diam}(K)) \max_{E \subset \partial K} \|\mathbf{n}_E \cdot \nabla u_K^h\|_E,$$

where $\|\cdot\|_E$ denotes the jump of a function across the face E and \mathbf{n}_E is a normal vector on E . This parameter has two user-chosen constants C_0 and C_1 . In BH04, the first term in the parentheses is negligible for small time steps.

In [10], it was proposed to choose (BE05_1)

$$\Psi_K(u_K^h)|_E = C \frac{\|\mathbf{C}\|_2 [\text{diam}(K)]^2 + \rho |R| [\text{diam}(K)]^3}{|K|} \|\nabla u_K^h\|_E \quad \forall E \subset \partial K.$$

Here, ρ is a measure of the local quasi-uniformity of the grid. The numerical examples in Section 7 were computed on uniform meshes, on which $\rho = 2$ can be chosen. The second term in the nominator of BE05_1 will dominate for small time steps.

Another proposal for the parameter function was considered in [34] (BE05_2)

$$\Psi_K(u_K^h)|_K = C |R^h(u_K^h)|_K.$$

The length of the time step influences this parameter only indirectly over the residual.

4.4. General remarks

All SOLD methods save JSW87 are non-linear methods. Thus, instead of solving a linear equation at t_k , a non-linear equation has to

be solved. This gives rise to questions like existence and uniqueness of a solution and the convergence of iterative solution schemes. With respect to these questions, even for the steady-state equations without reaction, only few results are known [42,21,10].

All non-linear SOLD methods which involve the computation of the residual require the storage of u_{k-1}^h and f_{k-1}^h (if $\theta_3 \neq 0$) during the whole iteration for solving the non-linear problem. If the data and the solutions vary only slowly with respect to the length of the time step, a good approximation of the residual is

$$u_k - u_{k-1} + \Delta t_k (-\varepsilon \Delta u_k + \mathbf{b} \cdot \nabla u_k + c u_k) - \Delta t_k f_k.$$

In the simulations presented in this paper, the residual computed with (2) was used.

5. Local projection stabilization schemes

The goal of local projection stabilization schemes consists in adding an appropriate stabilization to small scales of the finite element solution only. This approach is related to the idea of variational multiscale methods for the simulation of multiscale phenomena [29,25], for instance for the simulation of turbulent flows [28,32,33,31]. The scale separation in local projection methods is performed with local projections into a large scale space. This approach requires the use of two finite element spaces. They can be defined on different grids leading to a two-level method [3,5], see also [6] for a review, or on the same grid with higher order finite element functions leading to a one-level method, the so-called LPS method with enrichment [51,50,23]. The numerical studies will consider one type of a LPS scheme with enrichment.

The considered LPS method adds a linear term of the form

$$\sum_{K \in \mathcal{T}^h} \rho_K (\kappa^h(\nabla u^h), \kappa^h(\nabla v^h))_K$$

to the left hand side of the Galerkin finite element method (6). Let $id : L^2(\Omega) \rightarrow L^2(\Omega)$ be the identity map in $L^2(\Omega)$ and $\Pi_K : L^2(K) \rightarrow D^h(K)$ be the local L^2 -projection into the local coarse finite element space $D^h(K)$. Then the global projection is given by

$$\Pi^h : L^2(\Omega) \rightarrow D^h, \quad (\Pi^h v)|_K = \Pi_K(v|_K).$$

Now, the flux operator in the term which is introduced by the LPS scheme is defined by $\kappa^h := id - \Pi^h$. The analysis of steady-state convection–diffusion–reaction equations in [50] leads to the optimal parameter choice $\rho_K = C \text{diam}(K)$, where C is a user-chosen constant.

6. Finite element method – flux corrected transport schemes

FEM-FCT schemes have been developed in [48,46,45,44,43] for transport equations, i.e., equations of form (1) with $\varepsilon = c = f = 0$. These schemes do not modify the bilinear form which defines the finite element method, like SUPG, SOLD or LPS schemes. FEM-FCT schemes work on the algebraic level and they modify the system matrix and the right hand side vector. The description of FEM-FCT schemes in this paper will include diffusion, reaction and a right hand side.

Starting point is the fractional-step θ -scheme and the Galerkin FEM which leads to (6). The matrix–vector form of this equation is

$$(M_C + \theta_1 \Delta t_k A) u_k = (M_C - \theta_2 \Delta t_k A) u_{k-1} + \theta_3 \Delta t_k f_{k-1} + \theta_4 \Delta t_k f_k, \quad (21)$$

where $(M_C)_{ij} = (\varphi_j, \varphi_i)$ is the consistent mass matrix. The matrix A is the sum of diffusion, convection and reaction. The notations u_k, f_k etc. stand for the vectors of the unknown coefficients of the finite element method. As mentioned already, the solution of (21) shows huge spurious oscillations in many cases.

The first goal of FEM-FCT methods is as follows. If the maximum principle holds for the continuous Eq. (1), then this principle

should be inherited also from the discrete equation. This is given if the system matrix of the discrete equation is an M -matrix. A sufficient condition for a matrix to be an M -matrix is that all diagonal entries are positive, all off-diagonal entries are non-positive and the row sums are positive. Thus, FEM-FCT schemes proceed by defining the matrices

$$\begin{aligned} L &= A + D, \\ D &= (d_{ij}), \\ d_{ij} &= -\max\{0, a_{ij}, a_{ji}\} = \min\{0, -a_{ij}, -a_{ji}\} \quad \text{for } i \neq j, \\ d_{ii} &= -\sum_{j=1, j \neq i}^N d_{ij}, \end{aligned} \tag{22}$$

$$M_L = \text{diag}(m_i), \quad m_i = \sum_{j=1}^N m_{ij}, \tag{23}$$

where N is the number of degrees of freedom. The row and column sums of D are zero. The matrix L does not possess positive off-diagonal entries and the diagonal matrix M_L is called lumped mass matrix. Instead of (21), the equation

$$(M_L + \theta_1 \Delta t_k L) u_k = (M_L - \theta_2 \Delta t_k L) u_{k-1} + \theta_3 \Delta t_k f_{k-1} + \theta_4 \Delta t_k f_k \tag{24}$$

is considered. This is the algebraic representation of a stable low order scheme. The solution of (24) does not show spurious oscillations, however layers will be smeared because the operator on the left hand side is too diffusive.

The second goal of FEM-FCT schemes consists in modifying the right hand side of (24) such that the equation becomes less diffusive but spurious oscillations are still suppressed

$$(M_L + \theta_1 \Delta t_k L) u_k = (M_L - \theta_2 \Delta t_k L) u_{k-1} + \theta_3 \Delta t_k f_{k-1} + \theta_4 \Delta t_k f_k + f^*(u_k, u_{k-1}). \tag{25}$$

The ansatz for the vector $f^*(u_k, u_{k-1})$ uses the residual vector of (24) and (21)

$$\begin{aligned} r &= (M_L + \theta_1 \Delta t_k L - (M_C + \theta_1 \Delta t_k A)) u_k \\ &\quad - (M_L - \theta_2 \Delta t_k L - (M_C - \theta_2 \Delta t_k A)) u_{k-1} \\ &= (M_L - M_C)(u_k - u_{k-1}) + \Delta t_k D(\theta_1 u_k + \theta_2 u_{k-1}). \end{aligned}$$

The residual vector has to be weighted appropriately.

To define the weights, the residual vector is decomposed into fluxes r_{ij} , $i, j = 1, \dots, N$, in the following way

$$\begin{aligned} r_i &= \sum_{j=1}^N r_{ij} = \sum_{j=1}^N [m_{ij}(u_{k,i} - u_{k,j}) - m_{ij}(u_{k-1,i} - u_{k-1,j}) \\ &\quad - \Delta t_k \theta_1 d_{ij}(u_{k,i} - u_{k,j}) - \Delta t_k \theta_2 d_{ij}(u_{k-1,i} - u_{k-1,j})], \end{aligned} \tag{26}$$

$i = 1, \dots, N$. The derivation of this representation uses (22) and (23). The ansatz for the correction vector is now

$$f_i^*(u_k, u_{k-1}) = \sum_{j=1}^N \alpha_{ij} r_{ij}, \quad i = 1, \dots, N$$

with the weights $\alpha_{ij} \in [0, 1]$. If they depend on the residual vector then $f^*(u_k, u_{k-1})$ becomes a non-linear contribution. If all weights are equal to 1, the Galerkin finite element method is recovered.

6.1. A non-linear FEM-FCT scheme

The non-linear FEM-FCT scheme computes an explicit low order solution \tilde{u} at the time $t_{k-\theta_1} = t_k - \theta_1 \Delta t_k$. For the backward Euler scheme, $\tilde{u} = u_{k-1}$, whereas for the Crank–Nicolson scheme, this explicit solution is computed with the forward Euler scheme in (24), i.e. $\theta_1 = \theta_4 = 0$, $\theta_2 = \theta_3 = 1$, and the time step $\Delta t_k/2$

$$\tilde{u} = u_{k-1} - \frac{\Delta t_k}{2} M_L^{-1} (L u_{k-1} - f_{k-1}). \tag{27}$$

In the case of transport equations, \tilde{u} is a non-oscillating solution if the time step Δt_k is sufficiently small. The non-oscillating auxiliary solution \tilde{u} will be used for deciding in which regions the additional diffusion in (25) can be removed (setting α_{ij} close to 1) and in which regions this diffusion is necessary (setting α_{ij} close to 0), see Section 6.3.

6.2. A linear FEM-FCT scheme

A linear FEM-FCT scheme was presented recently in [43]. Consider the Crank–Nicolson scheme for discretizing the convection–diffusion–reaction Eq. (1), the residual flux defined in (26) becomes

$$\begin{aligned} r_{ij} &= m_{ij}(u_{k,i} - u_{k-1,i}) - m_{ij}(u_{k,j} - u_{k-1,j}) - \frac{\Delta t_k}{2} d_{ij}(u_{k,i} + u_{k-1,i}) \\ &\quad + \frac{\Delta t_k}{2} d_{ij}(u_{k,j} + u_{k-1,j}). \end{aligned} \tag{28}$$

The idea of the linear FEM-FCT consists in replacing u_k in (28) by an approximation which can be computed with an explicit scheme. To this end, define the intermediate value

$$u_{k-1/2} := \frac{u_k + u_{k-1}}{2}.$$

Inserting this value into (28) gives

$$\begin{aligned} r_{ij} &= 2m_{ij}(u_{k-1/2,i} - u_{k-1,i}) - 2m_{ij}(u_{k-1/2,j} - u_{k-1,j}) \\ &\quad - \Delta t_k d_{ij}(u_{k-1/2,i} - u_{k-1/2,j}). \end{aligned} \tag{29}$$

An approximation of $u_{k-1/2}$ can be obtained with the forward Euler scheme applied in the low order method (24) with time step $\Delta t_k/2$, see (27) for the solution \tilde{u} . Inserting this approximation into (29) leads to the fluxes in the linear FEM-FCT scheme

$$r_{ij} = \Delta t_k [m_{ij}(v_{k-1/2,i} - v_{k-1/2,j}) - d_{ij}(\tilde{u}_i - \tilde{u}_j)]$$

with

$$v_{k-1/2,i} = (M_L^{-1}(f_{k-1} - L u_{k-1}))_i, \quad \tilde{u}_i = u_{k-1,i} + \frac{\Delta t_k}{2} v_{k-1/2,i}.$$

6.3. Computation of the weights

For computing the weights, Zalesak’s algorithm [56] is used. The motivations for this algorithm are discussed in [44]. Here, we will give this algorithm for completeness of presentation:

(1) compute

$$P_i^+ = \sum_{j=1, j \neq i}^N \max\{0, r_{ij}\}, \quad P_i^- = \sum_{j=1, j \neq i}^N \min\{0, r_{ij}\},$$

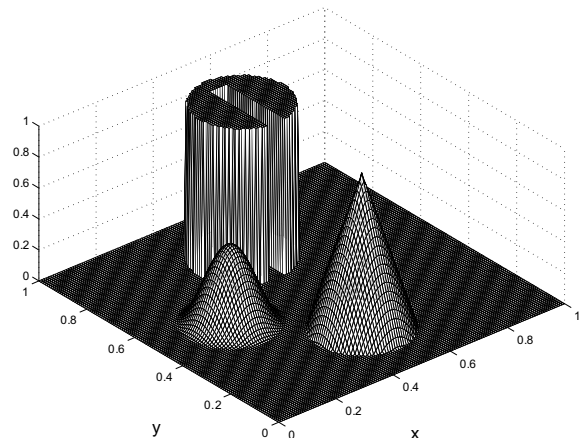


Fig. 4. Initial condition for rotating body problem.

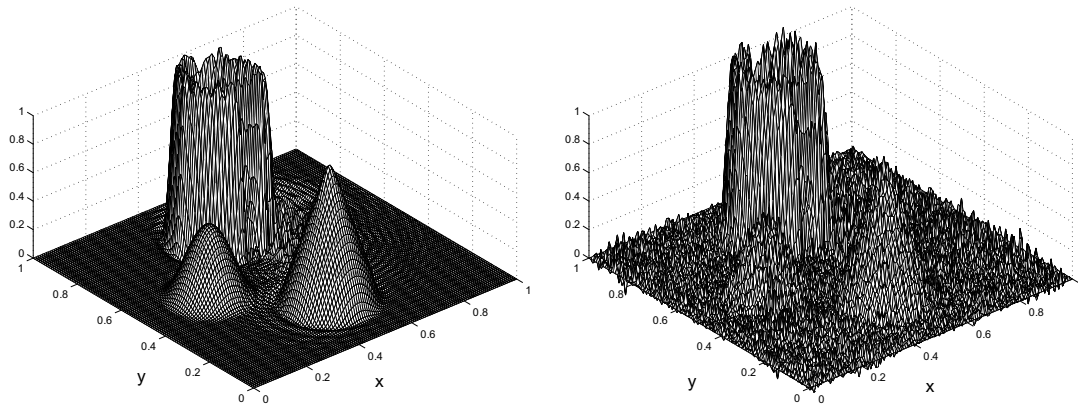


Fig. 5. SUPG solution obtained with parameter (11) [42,49] (left) and parameter (31) (right).

(2) compute

$$Q_i^+ = \max \left\{ 0, \max_{j=1, \dots, N, j \neq i} (\tilde{u}_j - \tilde{u}_i) \right\}, \quad Q_i^- = \min \left\{ 0, \min_{i=1, \dots, N, j \neq i} (\tilde{u}_j - \tilde{u}_i) \right\},$$

(3) compute

$$R_i^+ = \min \left\{ 1, \frac{m_i Q_i^+}{P_i^+} \right\}, \quad R_i^- = \min \left\{ 1, \frac{m_i Q_i^-}{P_i^-} \right\},$$

(4) compute

$$\alpha_{ij} = \begin{cases} \min\{R_i^+, R_j^-\} & \text{if } r_{ij} > 0, \\ \min\{R_i^-, R_j^+\} & \text{otherwise.} \end{cases}$$

Remark. Initially, the matrices M_C and A have to be assembled without any modifications for Dirichlet nodes. These modifications should be performed after having computed $f^*(u_k, u_{k-1})$. It is recommended to set $R_i^+ = R_i^- = 1$ if i corresponds to a Dirichlet node.

Remark. If $\theta_2 = \theta_3 = 1/2$, the first two terms in the right hand side of (25) can be computed by $M_L \tilde{u}$, such that the right hand side becomes

Table 1
Body rotation problem, results obtained with Q_1 (or Q_1^{bubble}/P_0 for the LPS scheme)

Method	$\ e^h\ _{L^2(L^2)}$	var(6.28)	Time	Damp.
SUPG (9) [15]	0.1517	1.5603	2618	–
SUPG (10) [20]	0.1517	1.5603	2624	–
SUPG (11) [42,49]	0.1515	1.5567	2618	–
GdC88 [22]	0.1516	1.5567	20,041	0.75
dCG91 [19]	Not converged			0.25
AS97 [1]	Not converged			0.25
dCA03 [18]	0.1516	1.5567	20,658	0.75
YZ β [54,2], iso	0.1987	0.9300	143,535	0.25
YZ β [54,2], aniso	0.1664	1.2873	19,809	1.0
C93 [13], C = 0.1	0.1493	1.3990	9726	1.0
C93 [13], C = 0.2	0.1536	1.3526	12,422	1.0
C93 [13], C = 0.3	0.1597	1.3162	14,822	1.0
C93 [13], C = 0.4	0.1666	1.2841	17,979	1.0
C93 [13], C = 0.5	0.1735	1.2546	23,475	1.0
C93 [13], C = 0.6	0.1800	1.2265	30,403	0.75
C93 [13], C = 0.7	0.1875	1.2002	33,457	0.75
C93 [13], C = 0.8	0.1949	1.1754	36,769	0.75
C93 [13], C = 0.9	0.2011	1.1522	40,863	0.75
C93 [13], C = 1.0	0.2071	1.1288	50,854	0.75
KLR02 [42,34], C = 0.1	0.1493	1.3990	9501	1.0
KLR02 [42,34], C = 0.5	0.1735	1.2546	22,846	1.0
KLR02 [42,34], C = 1.0	0.2070	1.1289	50,693	0.75
BE02_1 [8]	0.1515	1.5560	7841	1.0
BE02_2 [8,34]	0.1502	1.5175	6962	1.0
JSW87 [41]	0.1901	1.3075	3054	–
LPS scheme [50], C = 0.01	0.1325	1.3845	4936	–
LPS scheme [50], C = 0.05	0.1431	1.2732	4981	–
LPS scheme [50], C = 0.1	0.1503	1.2023	4901	–
LPS scheme [50], C = 0.5	0.1821	1.1835	4891	–
LPS scheme [50], C = 1	0.2022	1.1815	4860	–
LPS scheme [50], C = 2	0.2236	1.1612	4801	–
LPS scheme [50], C = 5	0.2547	1.0501	4858	–
LPS scheme [50], C = 10	0.2835	0.9406	4832	–
FEM-FCT linear [43]	0.1866	1.0076	2613	–
FEM-FCT non-linear [45,44]	0.1397	1.0013	47,939	1.0

Table 2
Body rotation problem, results obtained with P_1 (or P_1^{bubble}/P_0 for the LPS scheme)

Method	$\ e^h\ _{L^2(L^2)}$	var(6.28)	Time	Damp.
SUPG (9) [15]	0.1573	1.5299	2352	–
SUPG (10) [20]	0.1573	1.5299	2323	–
SUPG (11) [42,49]	0.1570	1.5275	2352	–
GdC88 [22]	0.1572	1.5280	17,552	0.75
dCG91 [19]	Not converged			0.25
AS97 [1]	Not converged			0.25
dCA03 [18]	0.1572	1.5280	17,283	0.75
YZ β [54,2], iso	Diverged			0.25
YZ β [54,2], aniso	0.1688	1.2471	15,749	1.0
C93 [13], C = 0.1	0.1549	1.3648	8487	1.0
C93 [13], C = 0.2	0.1595	1.3010	11,017	1.0
C93 [13], C = 0.3	0.1654	1.2590	13,972	1.0
C93 [13], C = 0.4	Diverged			0.25
KLR02 [42,34], C = 0.1	0.1549	1.3648	8251	1.0
KLR02 [42,34], C = 0.3	0.1654	1.2590	13,439	1.0
KLR02 [42,34], C = 0.4	0.1718	1.2183	16,468	1.0
KLR02 [42,34], C = 0.6	0.1852	1.1681	27,986	0.75
KLR02 [42,34], C = 0.8	0.1992	1.1215	38,207	0.75
KLR02 [42,34], C = 1.0	0.2121	1.0775	61,546	0.75
BE02_1 [8]	0.1570	1.5273	6499	1.0
BE02_2 [8,34]	0.1560	1.4956	5907	1.0
JSW87 [41]	0.1872	1.2877	2574	–
BH04 [11], $C_0 = C_1 = 1e - 4$	Diverged			0.25
BE05_1 [10], C = $1e - 5$	0.1536	1.3674	5610	1.0
BE05_1 [10], C = $1e - 4$	0.1615	1.0192	5672	1.0
BE05_1 [10], C = $1e - 3$	0.2881	0.7418	5632	1.0
BE05_2 [10,34], C = $1e - 4$	0.1543	1.3683	7465	1.0
BE05_2 [10,34], C = $1e - 3$	0.1703	1.0169	7479	1.0
BE05_2 [10,34], C = $1e - 2$	0.2998	0.7268	7527	1.0
LPS scheme [50], C = 0.01	0.1453	1.3818	6678	–
LPS scheme [50], C = 0.05	0.1517	1.5368	6703	–
LPS scheme [50], C = 0.1	0.1566	1.5667	6606	–
LPS scheme [50], C = 0.5	0.1667	1.7205	6582	–
LPS scheme [50], C = 1	0.1698	1.7605	6608	–
LPS scheme [50], C = 2	0.1723	1.7887	6602	–
LPS scheme [50], C = 5	0.1757	1.8212	6516	–
LPS scheme [50], C = 10	0.1782	1.8388	6516	–
FEM-FCT linear [43]	0.1920	1.0069	1912	–
FEM-FCT non-linear [45,44]	0.1439	1.0010	19,185	1.0

$$M_L \ddot{u} + \theta_4 \Delta t_k f_k + \left(\sum_{j=1}^N \alpha_{ij} r_{ij} \right)_{i=1, \dots, N}$$

Remark. The auxiliary solution \ddot{u} is used to guarantee the fulfillment of the maximum principle. Since \ddot{u} is computed with an explicit method, the stability of \ddot{u} gives rise to a CFL-like condition for FEM-FCT schemes. This condition is [44,43]

$$\Delta t_k < \frac{1}{\theta_2} \min_i \frac{m_i}{l_{ii}}. \tag{30}$$

Remark. The Crank–Nicolson scheme, $\theta_i = 0.5$, $i = 1, \dots, 4$, was used in the numerical studies of both types of FEM-FCT schemes presented in Section 7.

7. The numerical studies

The finite element methods presented in Sections 3–6 will be studied at examples given in a two-dimensional domain Ω . Standard benchmark problems for time-dependent scalar convection–diffusion–reaction equations do not seem to exist.

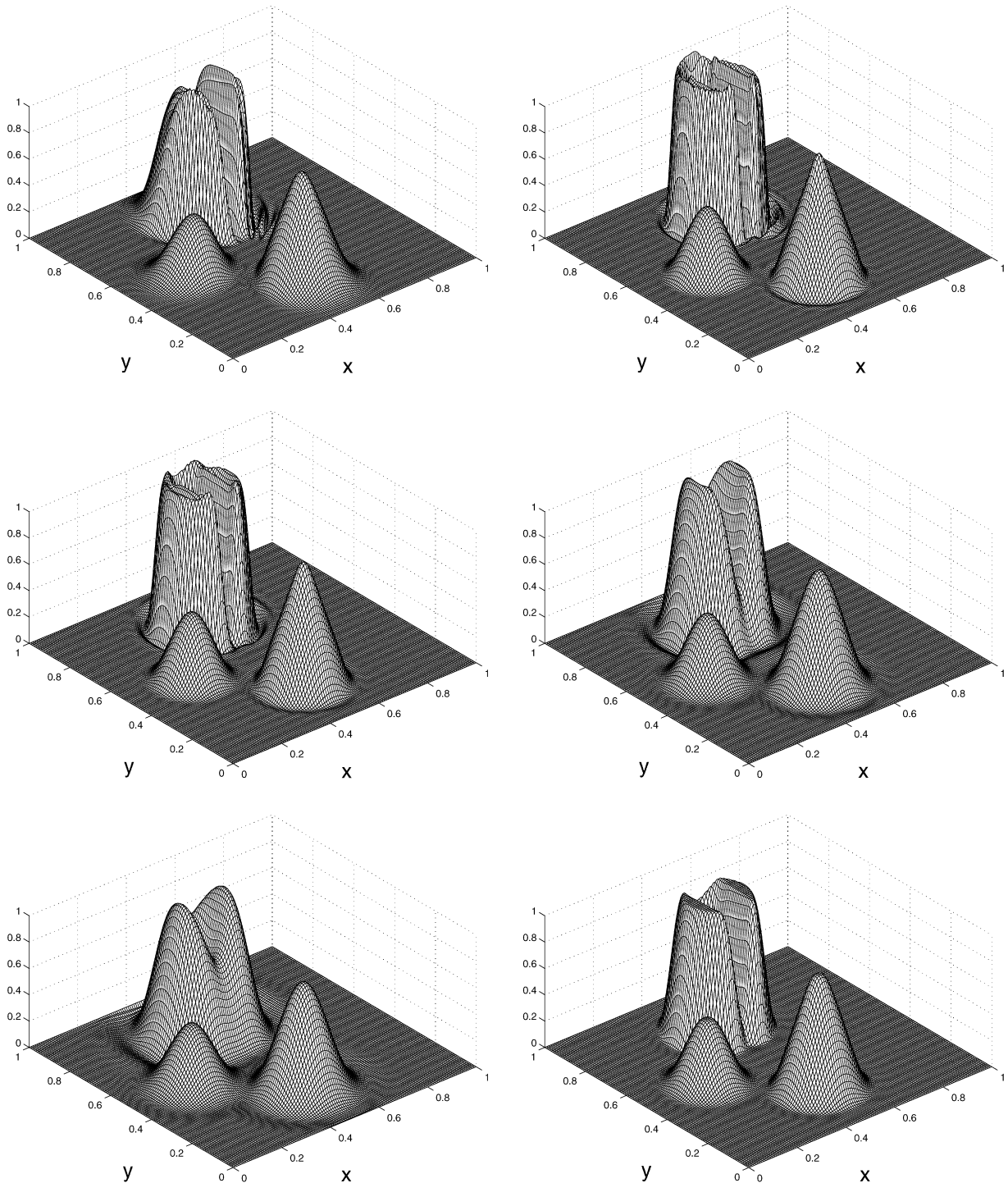


Fig. 6. Body rotation problem, the computed solution with Q_1 (or Q_1^{bubble}/P_0 for the LPS scheme) at $t = 6.28$; the linear schemes JWS87 [41], LPS scheme [50] with $C = 0.01$, $C = 0.1$, $C = 1$, $C = 5$, FEM-FCT linear [43]; from top left to bottom right.

The numerical studies are restricted to low order finite elements. This has several reasons. To our best knowledge, most of the SOLD methods and the LPS scheme have not yet been studied for time-dependent scalar convection–diffusion–reaction equations. Thus, it is natural to perform the first studies with the simplest finite elements. The final goal of our studies consists in identifying schemes which can be used in applications like in [39]. Many finite element codes which are used to simulate problems coming from applications are based on low order finite elements. For these reasons, apart from the LPS scheme, P_1 finite

elements were used on triangular meshes and Q_1 finite elements on quadrilateral grids.

As mentioned in Section 5, the LPS scheme requires two finite element spaces. The simplest large scale projection space D^h is the space of piecewise constant functions. To obtain a well-posed discrete problem, the fine scale finite element space V^h and the large scale projection space have to obey an inf-sup condition, see [51]. Unfortunately, this inf-sup condition is not satisfied by the spaces $V^h = P_1$ or $V^h = Q_1$. Appropriate spaces which fulfill the inf-sup condition have been identified in [51]. These are the

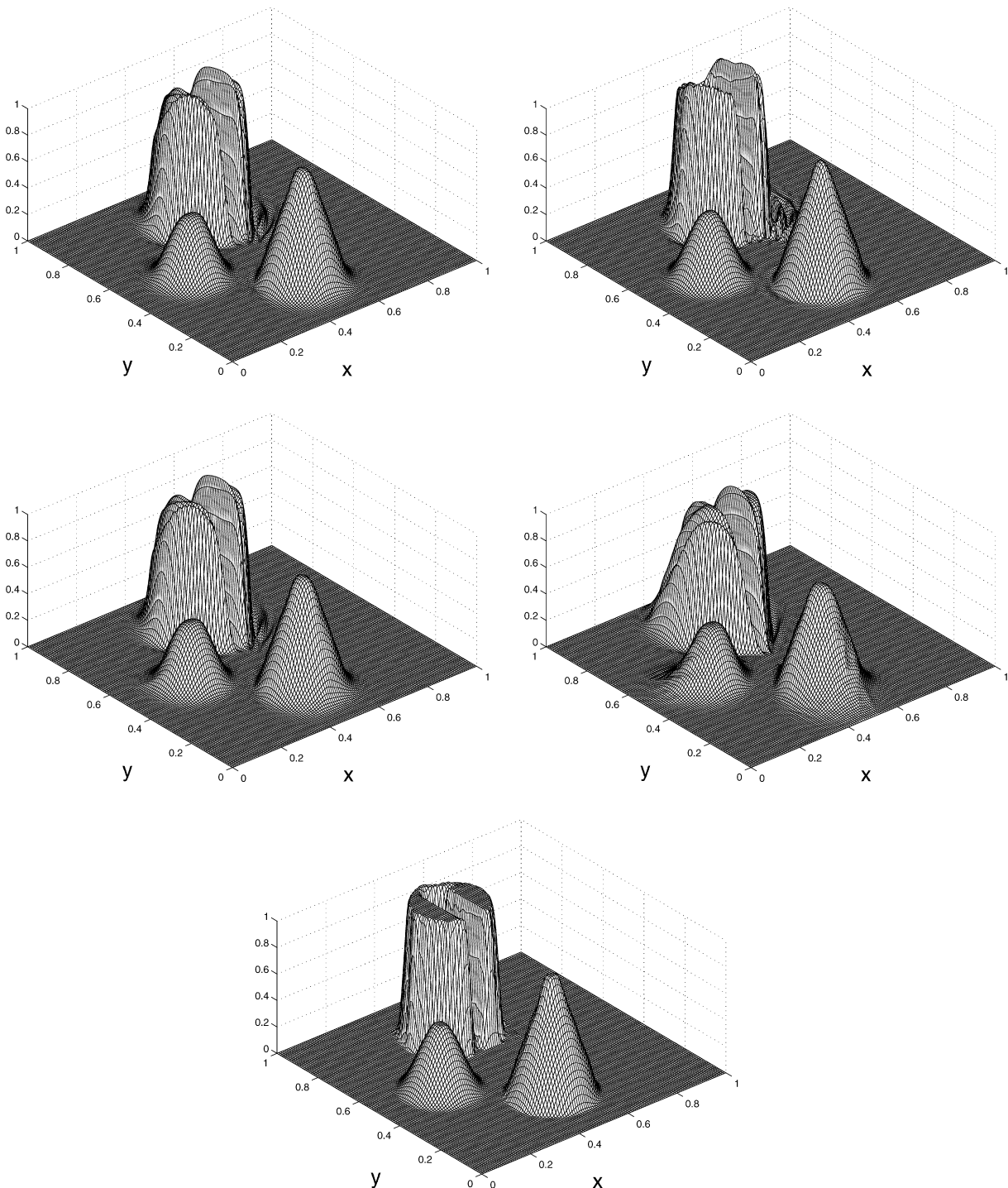


Fig. 7. Body rotation problem, the computed solution with Q_1 at $t = 6.28$; the non-linear schemes $YZ\beta$ [54,2] anisotropic, C93 [13] with $C = 0.1$, $C = 0.5$, $C = 1$ and FEM-FC non-linear [45,44]; from top left to bottom.

spaces $V^h/D^h = P_1^{\text{bubble}}/P_0$ and $V^h/D^h = Q_1^{\text{bubble}}/P_0$, i.e. the standard spaces P_1, Q_1 have to be enriched with bubble functions.

In all simulations with SUPG and SOLD schemes, the parameter h_K was chosen to be the mesh width of the mesh cell K in the direction of the convection, see the remark at the end of Section 3. The length of the mesh cell in the direction of the convection can be easily approximated, see [55,34]. The SUPG parameters (9)–(11) were scaled with the factor 1.

The non-linear problems for most of the SOLD methods and the non-linear FEM-FCT method were solved in each discrete time up

to the Euclidean norm of the residual vector less than 10^{-9} . A simple fixed point iteration was employed, see [36], with a fixed damping factor. Damping was only applied if the method without damping diverged (a blow-up occurred) or if it did not converge (the non-linear problems could not be solved to the required accuracy). In applications, it is of advantage if a method works without a sophisticated choice of the damping factor. We considered damping factors from the set $\{1, 0.75, 0.5, 0.25\}$, where we started with the largest factor. Only if the non-linear iteration did not work for the given factor, the simulations were repeated with the next

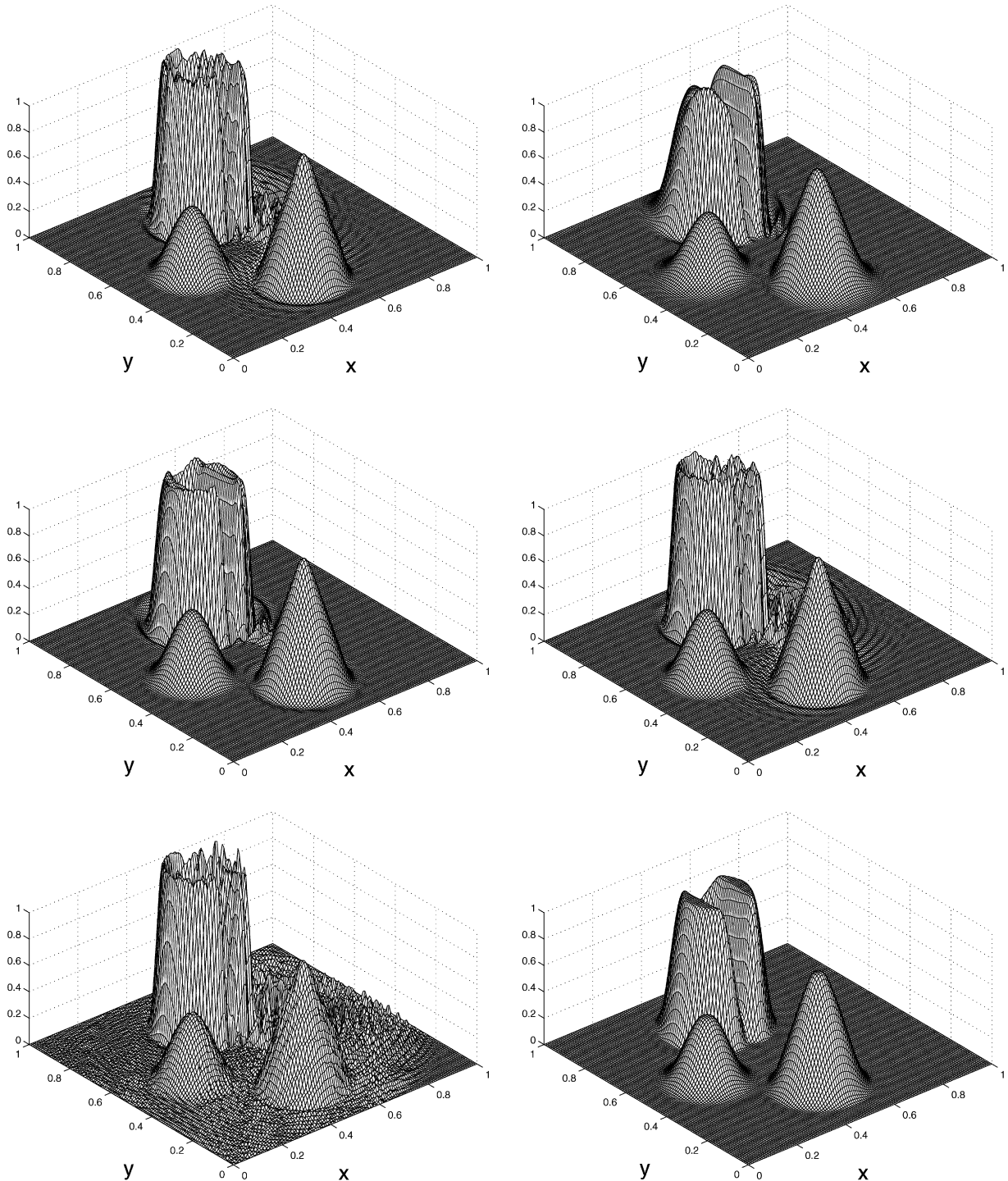


Fig. 8. Body rotation problem, the computed solution with P_1 (or P_1^{bubble}/P_0 for the LPS scheme) at $t = 6.28$; the linear schemes SUPG (11) [42,49], JWS87 [41], LPS scheme [50] with $C = 0.01, C = 0.1, C = 1$, FEM-FCT linear [43]; from top left to bottom right.

smaller damping factor. Smaller damping factors than 0.25 would lead to a very large number of iterations to solve the non-linear problems and thus to inefficient methods. The maximal number of iterations in each discrete time was set to be 100. The matrices were assembled in each iteration, which will be also necessary in the simulation of chemical reactions.

A lot of studies would have been possible with respect to the used meshes and time steps. To keep the paper at a reasonable length, we restricted the studies to the situation which occurs in the simulation of precipitation processes [39]: rather small time steps and grid sizes of medium range. It was checked numerically

that the used time steps and grid sizes fulfill the CFL-like condition (30) for the FEM-FCT methods.

All simulations were performed with the code MoonMD [37]. The linear systems of equations were solved with the sparse direct solver UMFPACK [17].

7.1. A body rotation problem

The first example is an adaption of the three body rotation transport problem from [47]. This problem with $\varepsilon = 0$ was extensively studied in simulations with flux corrected transport finite

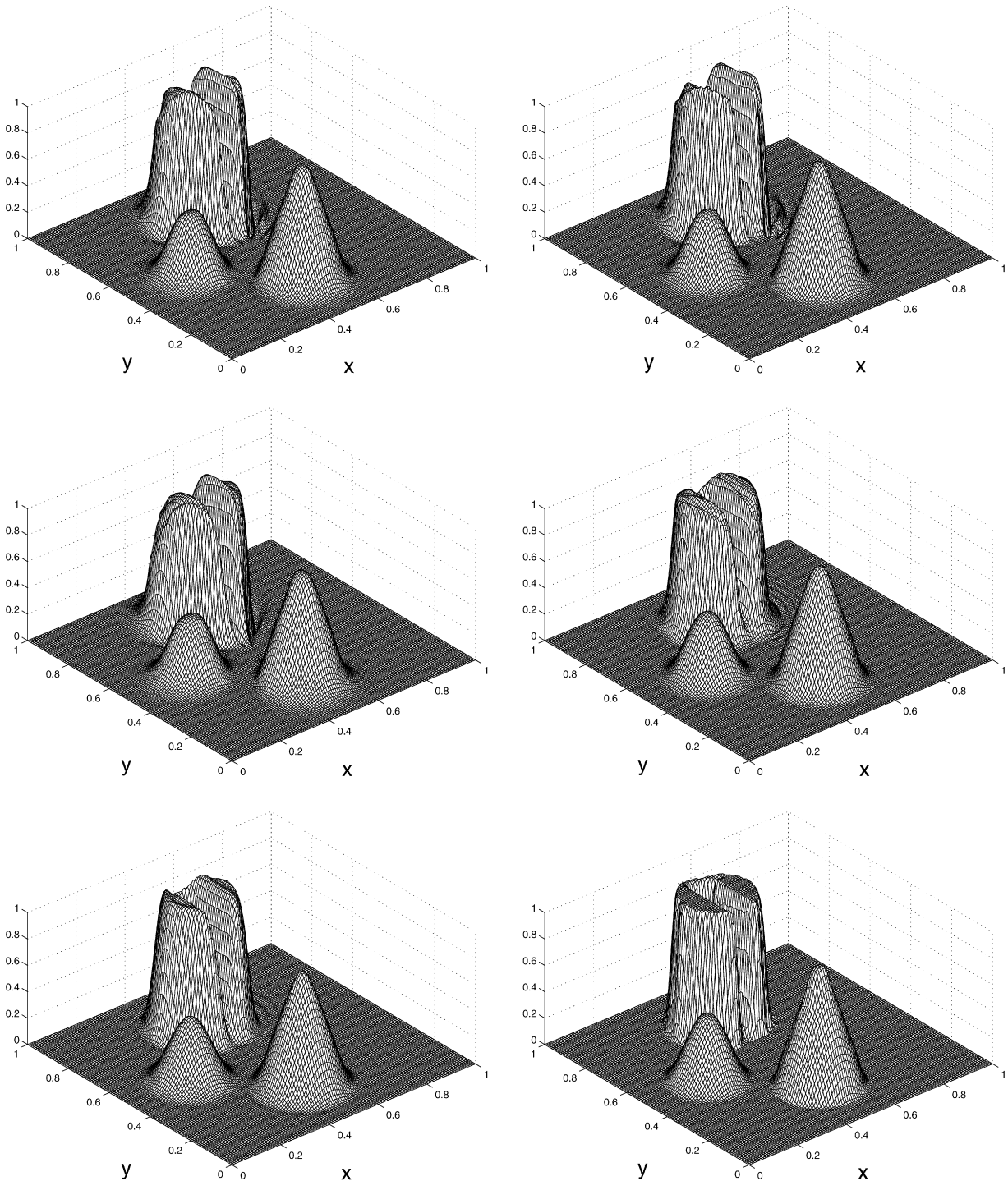


Fig. 9. Body rotation problem, the computed solution with P_1 at $t = 6.28$; the non-linear schemes $YZ\beta$ [54,2] anisotropic, KLR02 [42,34] with $C = 0.2$, $C = 0.6$, BE05_1 [10] with $C = 1e - 4$, BE05_2 [10,34] with $C = 1e - 3$ and FEM-FCT non-linear [45,44]; from top left to bottom right.

element methods [44,43]. A problem with circular convection was also considered in [4].

Consider (1) in $\Omega = (0, 1)^2$ with the coefficients $\varepsilon = 10^{-20}$, $\mathbf{b} = (0.5 - y, x - 0.5)^T$, $c = f = 0$. The initial condition consists of three disjoint bodies, see Fig. 4. The position of each body is given by its center (x_0, y_0) . Each of the bodies lies within a circle of radius $r_0 = 0.15$ with the center (x_0, y_0) . Outside the three bodies, the initial condition is zero.

Let

$$r(x, y) = \frac{1}{r_0} \sqrt{(x - x_0)^2 + (y - y_0)^2}.$$

The center of the slotted cylinder is in $(x_0, y_0) = (0.5, 0.75)$ and its geometry is given by

$$u(0; x, y) = \begin{cases} 1 & \text{if } r(x, y) \leq 1, |x - x_0| \geq 0.0225 \text{ or } y \geq 0.85, \\ 0 & \text{else.} \end{cases}$$

The conical body at the bottom side is described by $(x_0, y_0) = (0.5, 0.25)$ and

$$u(0; x, y) = 1 - r(x, y).$$

Finally, the hump at the left hand side is given by $(x_0, y_0) = (0.25, 0.5)$ and

$$u(0; x, y) = \frac{1}{4} (1 + \cos(\pi \min\{r(x, y), 1\})).$$

The rotation of the bodies occurs counter-clockwise. A full revolution takes $t = 2\pi$. The original example from [47] is a pure transport problem, i.e. $\varepsilon = 0$, and ideally one should obtain the initial condition after each revolution. But even with the very small diffusion ε used in our numerical studies, an ideal method should give a result which is very close to the initial condition.

In the simulations, regular grids consisting of 128×128 triangular or rectangular (squared) mesh cells were used. This is the same grid size which was applied in [44,43]. The number of degrees of freedom, including Dirichlet nodes, is 16,641. For the LPS scheme, the numbers of degrees of freedom are 33,025/16,384 for Q_1^{bubble}/P_0 and 49,409/32,768 for P_1^{bubble}/P_0 . In the triangular

Table 3
Hump changing its height, results obtained with Q_1 (or Q_1^{bubble}/P_0 for the LPS scheme)

Method	$\ e_h\ _{L^2(\Omega^h)}$	var(0.5)	Time	Damp.
SUPG (9) [15]	11.2143	1.4282	5297	–
SUPG (10) [20]	11.2142	1.4281	5275	–
SUPG (11) [42,49]	10.4631	1.3287	5245	–
GdC88 [22]	10.4631	1.3287	10,133	1.0
dCG91 [19]	Not converged			0.25
AS97 [1]	Not converged			0.25
dCA03 [18]	10.4631	1.3287	14,824	1.0
YZ β [54,2], iso	Diverged			0.25
YZ β [54,2], aniso	9.9861	1.1566	56,944	1.0
C93 [13], C = 0.1	10.0980	1.2382	39,826	1.0
C93 [13], C = 0.2	9.9485	1.1902	131,413	0.75
KLR02 [42,34], C = 0.1	10.0987	1.2381	19,249	1.0
KLR02 [42,34], C = 0.2	9.9494	1.1901	22,284	1.0
KLR02 [42,34], C = 0.4	9.9334	1.1553	35,022	1.0
KLR02 [42,34], C = 0.6	10.1140	1.1347	56,608	1.0
KLR02 [42,34], C = 0.8	10.3289	1.1196	83,386	1.0
BE02_1 [8]	10.2129	1.2548	16,613	1.0
BE02_2 [8,34]	9.9418	1.2027	21,250	1.0
JSW87 [41]	9.9255	1.1986	6300	–
LPS scheme [50], C = 0.01	30.1938	1.4198	6016	–
LPS scheme [50], C = 0.05	14.1264	1.3689	6017	–
LPS scheme [50], C = 0.1	11.5793	1.3528	6012	–
LPS scheme [50], C = 0.5	10.5392	1.3432	6026	–
LPS scheme [50], C = 1	11.2444	1.4474	6013	–
LPS scheme [50], C = 5	12.6169	1.5109	6093	–
FEM-FCT linear [43]	9.6811	1.0101	2605	–
FEM-FCT non-linear [45,44]	9.4399	1.0240	10,051	1.0

grids, the diagonals of the triangles were from bottom left to top right. The simulations were performed with the final time $T = 6.28$ and the time step $\Delta t = 10^{-3}$. The numerical solutions were compared with the appropriately rotated initial condition $u(t)$. Denote the error by $e^h = u - u^h$. We present $\|e^h\|_{L^2(\Omega)} := \|e^h\|_{L^2(0,T;L^2(\Omega))}$ and

$$\text{var}(t) := \max_{(x,y) \in \Omega} u^h(t; x, y) - \min_{(x,y) \in \Omega} u^h(t; x, y),$$

where the maximum and the minimum were computed in the vertices of the mesh cells. The values $\|e^h\|_{L^2(\Omega)}$ give some indication of the accuracy of the methods and the smearing in the numerical solutions whereas $\text{var}(t)$ measures the size of the spurious oscillations. The optimal value is $\text{var}(t) = 1$ for all $t \in [0, T]$.

First, it is demonstrated that the SUPG method has to be used with a parameter including a contribution from the reactive term. A standard parameter for steady-state convection–diffusion equations is

$$\tau_K^{cd} = \frac{h_K}{2\|\mathbf{b}\|_2} \xi(Pe_K), \quad Pe_K = \frac{\|\mathbf{b}\|_2 h_K}{2\varepsilon}, \quad \xi(\alpha) = \coth \alpha - \frac{1}{\alpha}. \quad (31)$$

Fig. 5 shows that the SUPG solution with the parameter (31) is globally polluted with large spurious oscillations whereas the solution obtained with the parameter (11) possesses large spurious oscillations only at the layers. The spurious oscillations are also considerably larger in the solution obtained with τ_K^{cd} .

The results of the computations on the rectangular grid are summarized in Table 1 and on the triangular grid in Table 2. Among the SUPG methods, the largest parameter (11) gave slightly better results than the parameters (9) and (10). All SOLD methods were used together with the SUPG parameter (11).

Table 4
Hump changing its height, results obtained with P_1 (or P_1^{bubble}/P_0 for the LPS scheme)

Method	$\ e_h\ _{L^2(\Omega^h)}$	var(0.5)	Time	Damp.
SUPG (9) [15]	13.3334	1.5022	8550	–
SUPG (10) [20]	13.3334	1.5022	8535	–
SUPG (11) [42,49]	12.1257	1.3835	8550	–
GdC88 [22]	12.1257	1.3835	16,331	1.0
dCG91 [19]	Not converged			0.25
AS97 [1]	Not converged			0.25
dCA03 [18]	12.1257	1.3835	24,513	1.0
YZ β [54,2], iso	Not converged			0.25
YZ β [54,2], aniso	10.3968	1.1620	153,748	1.0
C93 [13], C = 0.1	Diverged			0.25
KLR02 [42,34], C = 0.1	10.9608	1.2467	34,462	1.0
KLR02 [42,34], C = 0.2	10.5832	1.1970	48,901	1.0
KLR02 [42,34], C = 0.4	10.3922	1.1483	84,390	1.0
KLR02 [42,34], C = 0.6	10.5113	1.1279	104,510	1.0
KLR02 [42,34], C = 0.8	10.7120	1.1179	248,731	0.75
BE02_1 [8]	11.5072	1.2985	31,441	1.0
BE02_2 [8,34]	10.5888	1.2081	39,154	1.0
JSW87 [41]	10.4819	1.1992	10,163	–
BH04 [11], C ₀ = C ₁ = 1e – 4	Diverged			0.25
BE05_1 [10], C = 1e – 5	12.1116	1.3807	16,349	1.0
BE05_1 [10], C = 1e – 4	11.9987	1.3558	16,311	1.0
BE05_1 [10], C = 1e – 3	11.4126	1.2830	16,222	1.0
BE05_1 [10], C = 1e – 2	Diverged			0.25
BE05_2 [10,34], C = 1e – 4	12.1168	1.3821	17,379	1.0
BE05_2 [10,34], C = 1e – 3	12.0402	1.3695	17,376	1.0
BE05_2 [10,34], C = 1e – 2	11.4982	1.2634	17,150	1.0
BE05_2 [10,34], C = 1e – 1	10.9352	1.2079	17,109	1.0
BE05_2 [10,34], C = 1	Diverged			0.25
LPS scheme [50], C = 0.01	68.6146	1.2007	9683	–
LPS scheme [50], C = 0.05	19.9672	1.2964	9611	–
LPS scheme [50], C = 0.1	15.7470	1.4201	9650	–
LPS scheme [50], C = 0.5	19.8025	1.8261	9578	–
LPS scheme [50], C = 1	26.2342	1.9659	9614	–
LPS scheme [50], C = 2	35.6500	2.1306	9535	–
FEM-FCT linear [43]	9.8994	1.0134	3929	–
FEM-FCT non-linear [45,44]	9.8254	1.0225	9351	1.0

Remark. Numerical studies (not presented here) showed that decreasing the size of the time step, which might be necessary in the simulation of chemical reactions, gave similar solutions as presented in Fig. 5 (left picture). Only the size of the spurious oscillations increased somewhat. These observations are consistent to the analytical results of [4] concerning the stability of the SUPG method.

The best results in the body rotation problem were obtained with the non-linear FEM-FCT scheme, see Figs. 7 and 9. This is not surprising since this method was designed for transport problems. Also the linear FEM-FCT method suppressed spurious oscillations but led to some smearing, Figs. 6 and 8.

As expected, the methods GdC88 and dCA03 led to nearly the same results as the SUPG method. The non-linear iteration did not converge for the methods dCG91 and AS97. The use of the isotropic variant of the $YZ\beta$ scheme resulted in large difficulties in the solution of the non-linear problems. For the triangular discretization, this method even blew up for all considered damping parameters.

The increasing influence of the SOLD term can be observed clearly in the parameter studies for C93 and KLR02. Since D is very small in the rotating body problem, these methods gave nearly

identical results. Large parameters, which make the problems more non-linear, led on the one hand to smaller spurious oscillations and larger smearing, see Figs. 7 and 9. On the other hand, some damping in the non-linear iteration became necessary for

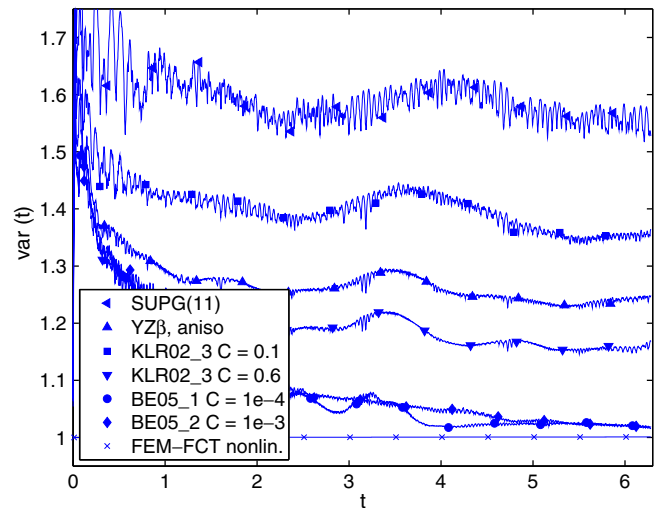
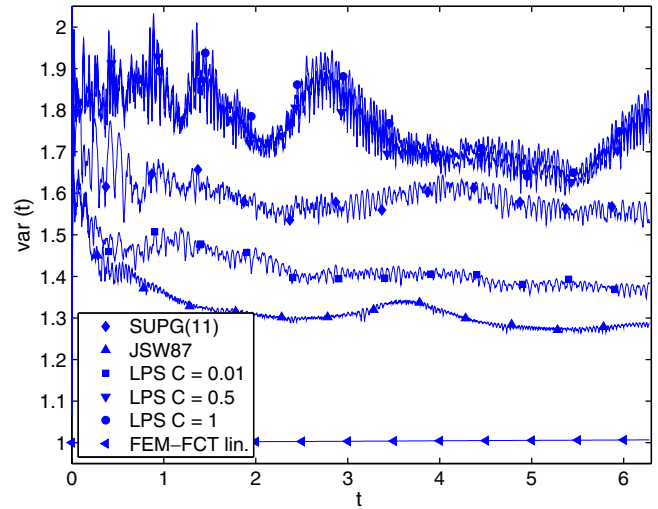


Fig. 11. Body rotation problem, evolution of $\text{var}(t)$ for the solutions computed with P_1 (or p_1^{bubble}/p_0 for the LPS scheme).

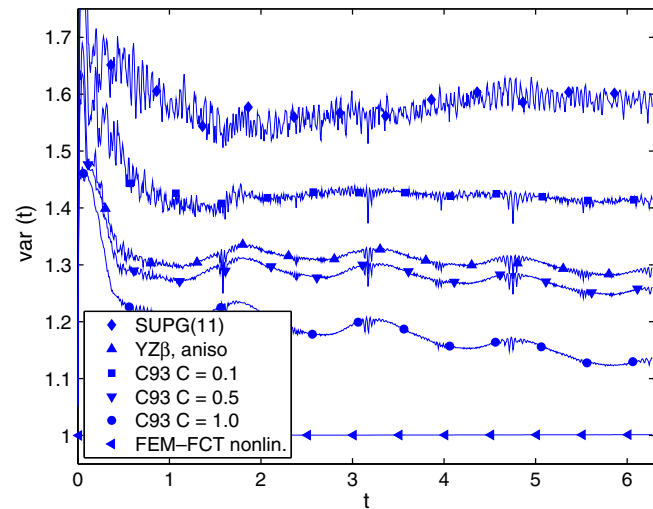
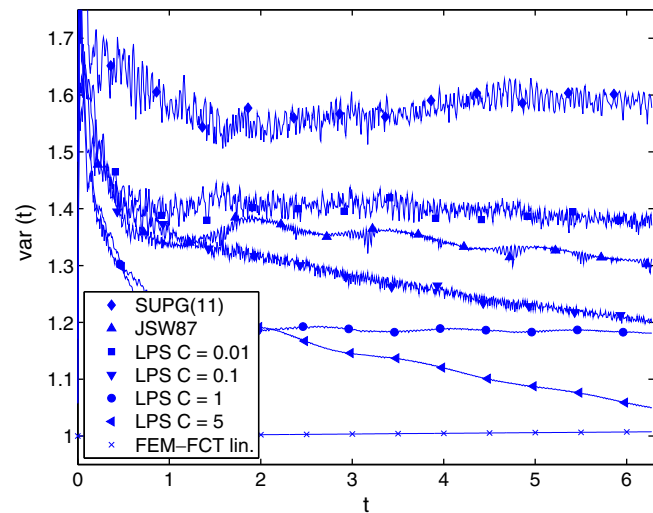


Fig. 10. Body rotation problem, evolution of $\text{var}(t)$ for the solutions computed with Q_1 (or Q_1^{bubble}/p_0 for the LPS scheme).

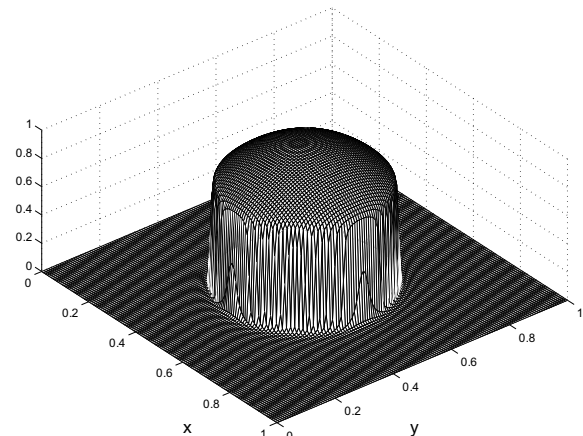


Fig. 12. A hump changing its height, solution at $t = 0.5$.

large parameters, the numbers of iterations to solve the non-linear problems and accordingly the computing times increased. It is hard to decide which is the best parameter choice if all aspects (spurious oscillations, smearing, computing times) are taken into consideration. The computations on the triangular grid show clearly the difficulties in the solution of the non-linear equations of C93 which arise from the non-linearity of the second term in (17).

As expected, the SOLD term in BE02_1 and BE02_2 had only little influence and one obtained similar results as with the SUPG method.

The linear SOLD scheme JSW87 tended to reduce the spurious oscillations but also to smear the discrete solution considerably.

For the edge stabilization method BH04, the iteration for solving the non-linear problems diverged even for very small user-chosen parameters C_0 and C_1 . The parameter studies of BE05_1 and BE05_2 show again that increasing the influence of the SOLD term reduced the spurious oscillations but smeared the solution.

The parameter study of the LPS scheme leads to different results for the quadrilateral and the triangular mesh. Increasing the parameter resulted on the quadrilateral mesh to less spurious

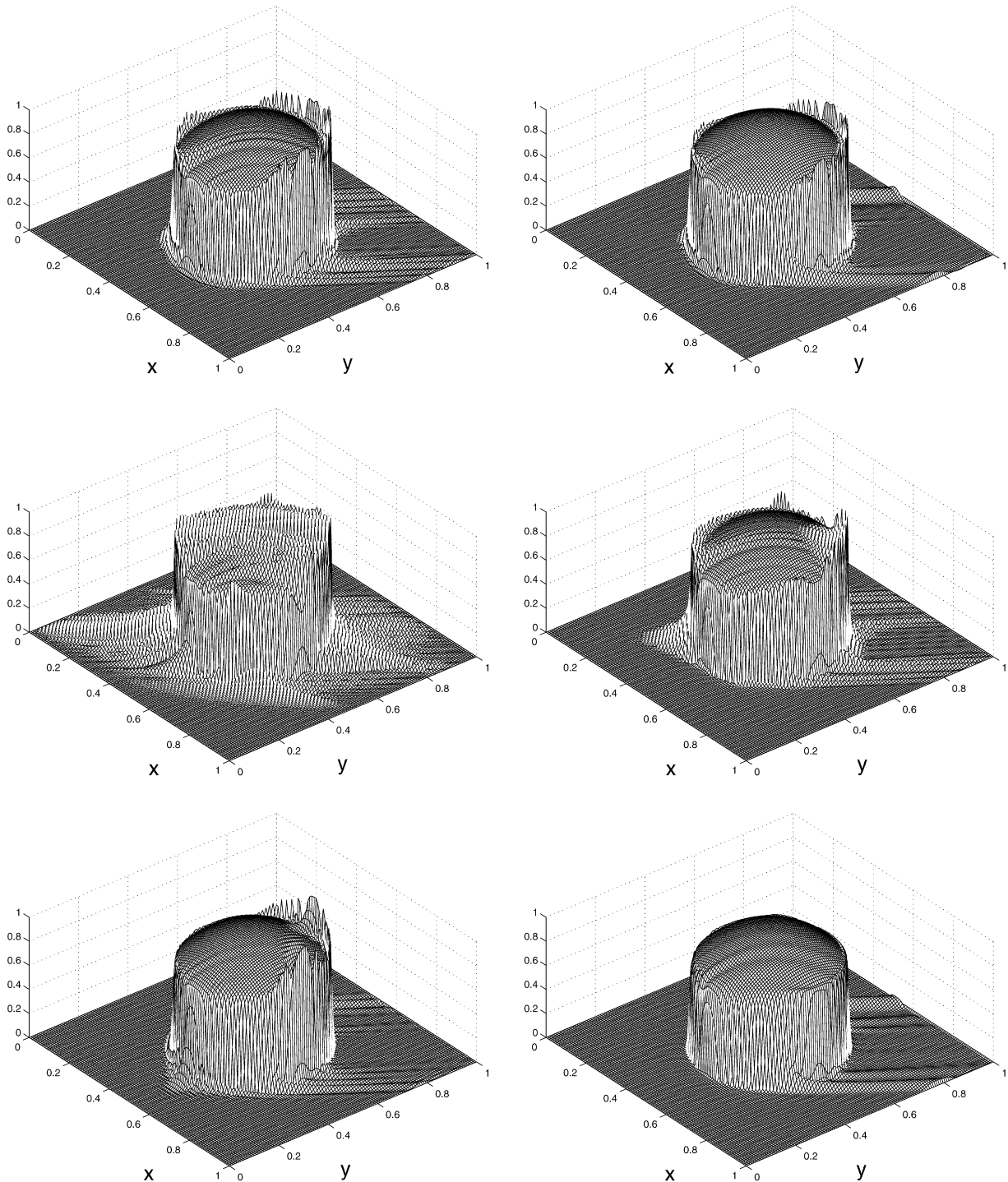


Fig. 13. Hump changing its height, the computed solution with Q_1 (or Q_1^{bubble}/P_0 for the LPS scheme) at $t = 0.5$; the linear schemes SUPG with (11) [42,49], JSW87 [41], LPS scheme [50] with $C = 0.01$, $C = 0.1$, $C = 1$, FEM-FCT linear [43]; from top left to bottom right.

oscillations and larger smearing, Table 1 and Fig. 6. This situation is vice versa on the triangular mesh, Table 2 and Fig. 8.

The temporal evolution of the spurious oscillations is illustrated in Figs. 10 and 11. For the FEM-FCT schemes, the value $\text{var}(t)$ was all the time close to the optimal value. Many schemes exhibited rather large spurious oscillations at the beginning of the time interval which were smoothed somewhat in later times. Among these schemes are JSW87, C93 and KLR02 for large parameters, $YZ\beta$ anisotropic and the LPS schemes on the quadrilateral grid.

7.2. A hump changing its height

This example is an adaption of Example 2 from [38] for the steady-state convection–diffusion–reaction equation. The prescribed solution has the form

$$u(t; x, y) = 16 \sin(\pi t) x(1-x)y(1-y) \times \left(\frac{1}{2} + \frac{\arctan[2\varepsilon^{-1/2}(0.25^2 - (x-0.5)^2 - (y-0.5)^2)]}{\pi} \right). \tag{32}$$

This is a hump changing its height in the course of the time, see Fig. 12 for the solution at $t = 0.5$. The steepness of the circular internal layer depends on the diffusion parameter ε . The thickness of the layer is $\sqrt{\varepsilon}$ which is typical for interior layers [52].

We present simulations for $\varepsilon = 10^{-6}$, $\mathbf{b} = (2, 3)$, $c = 1$ and $T = 2$. In contrast to the previous example, a reactive term of order 1 appears and the right hand side does not vanish. The time step was chosen to be $\Delta t = 10^{-3}$ and the computations were performed on the same grids as in Example 7.1. Hence, the convection is not aligned to the grid.

It is important to note that for the computation of this example very accurate quadrature rules, at least for the right hand side, are necessary. Since the solution possesses a steep layer, the right hand side has also regions with large gradients. We found that using low order quadrature rules leads to a strong pollution of the computed solutions with all schemes. For the results presented in this section, Gaussian quadrature which is exact for polynomials of degree 17 (81 quadrature points) was used on the quadrilateral mesh. On the triangular mesh, a quadrature rule which is exact for polynomials of degree 19 (73 quadrature points) was applied. Since in our code all matrices and vectors are assembled together, also the matrices have been assembled with the high order quadrature rule. The computing times given below are dominated by the costs of the numerical quadrature.

The variation of the discrete solutions at $t = 0.5$ (maximal height of the hump) was used for evaluating the size of the spurious oscillations. The value for (32) is $\text{var}(0.5) = 0.997453575$. We also monitored the variation of the discrete solution at the final time $T = 2$. For almost all schemes, we obtained $\text{var}(2) < 0.04$, i.e. rather small oscillations. For this reason, $\text{var}(2)$ is not reported

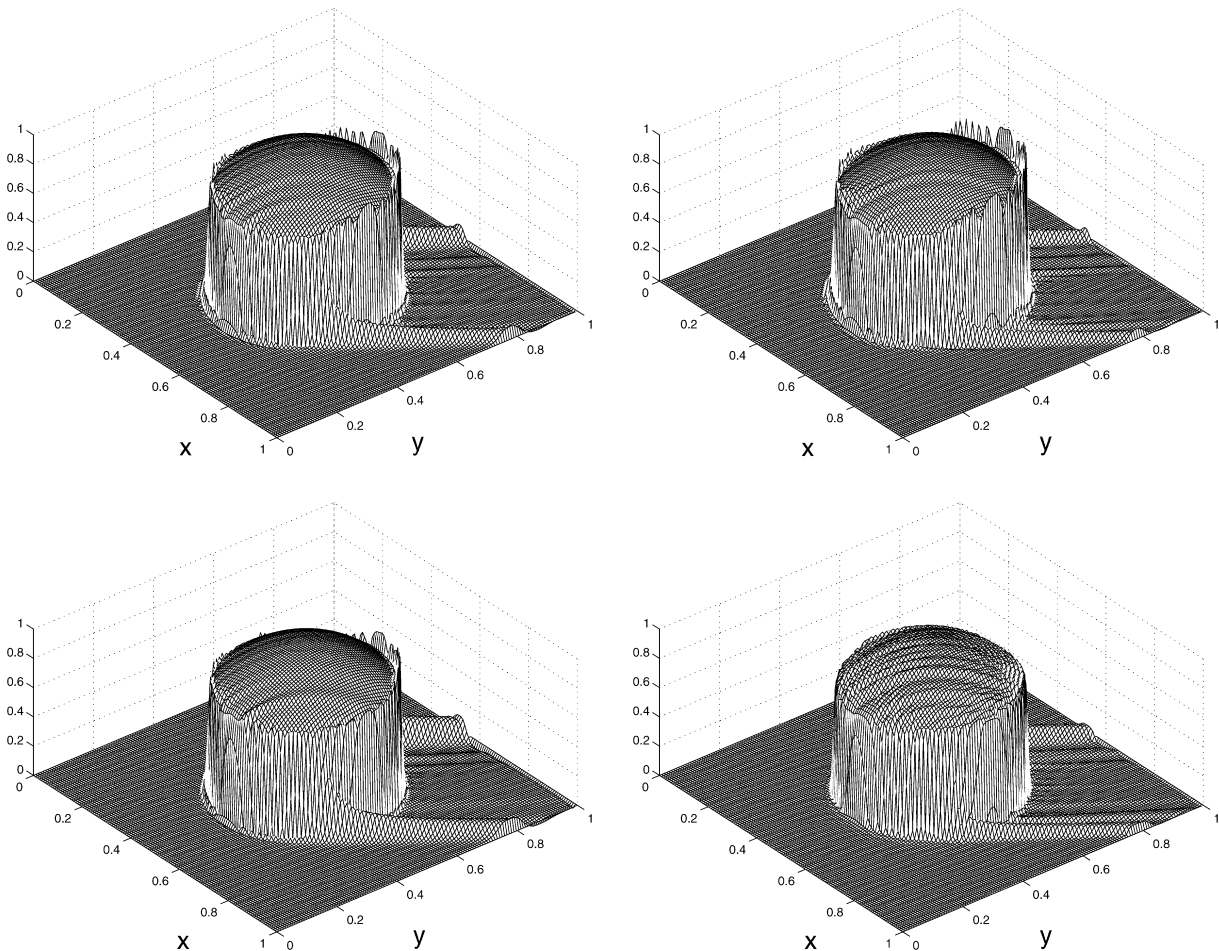


Fig. 14. Hump changing its height, the computed solution with Q_1 at $t = 0.5$; the non-linear schemes $YZ\beta$ [54,2] anisotropic, KLR02 [42,34] with $C = 0.2$, $C = 0.6$ and FEM-FCT non-linear [45,44]; from top left to bottom.

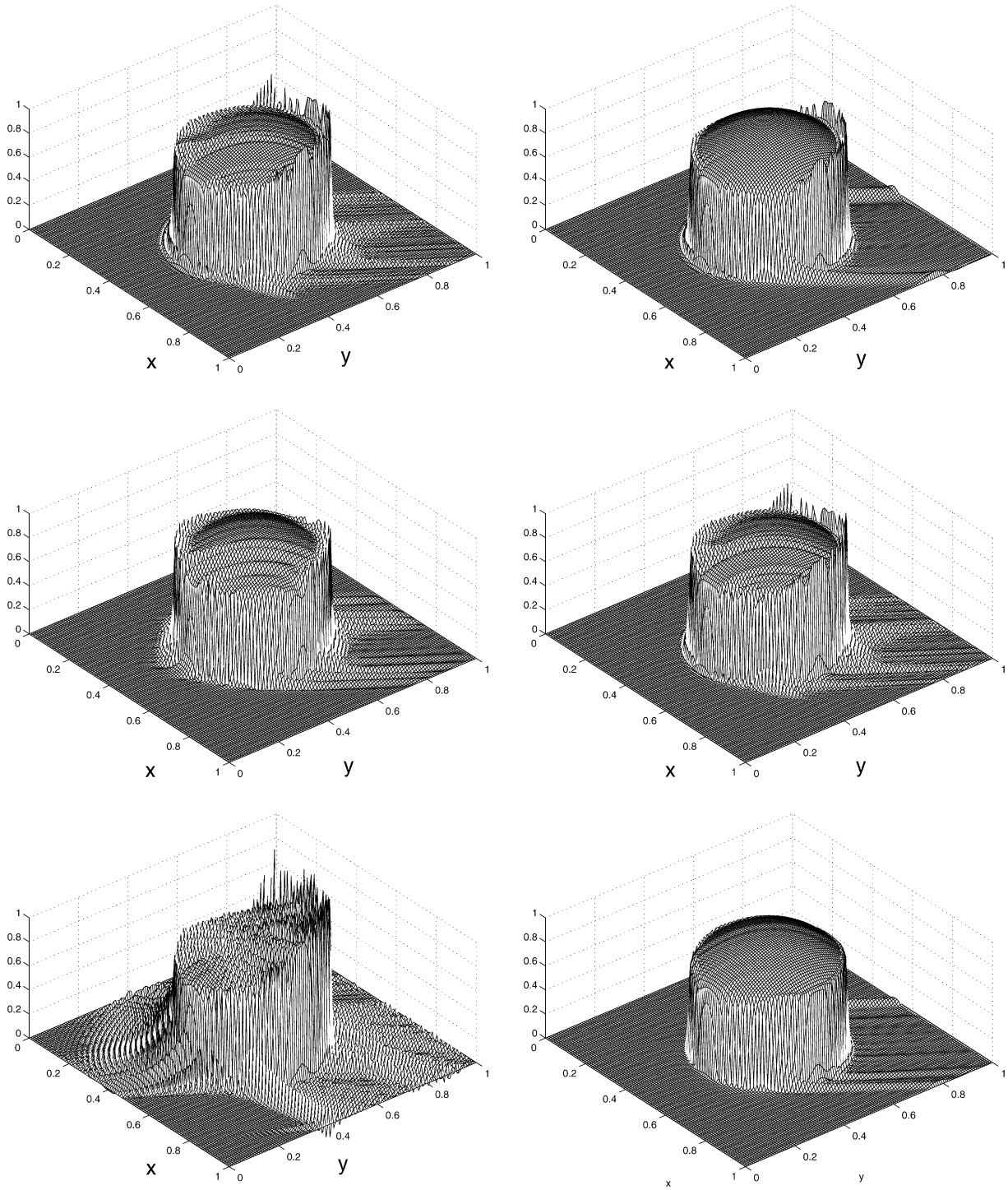


Fig. 15. Hump changing its height, the computed solution with P_1 (or P_1^{bubble}/P_0 for the LPS scheme) at $t = 0.5$; the linear schemes SUPG (11) [42,49], JSW87 [41], LPS scheme [50] with $C = 0.01$, $C = 0.1$, $C = 1$, FEM-FCT linear [43]; from top left to bottom right.

in the tables given below. An indication of the smearing of the solution is derived from $\|e_h\|_{L^2(H^1)} := \|\nabla e_h\|_{L^2(0,T;L^2(\Omega))}$. The simulations with the SOLD methods were based again on the SUPG parameter (11).

The results are presented in Tables 3 and 4 and in Figs. 13–16. It can be observed that all schemes led to spurious oscillations behind the hump in the direction of the convection. The only methods which suppressed spurious oscillations at the interior layer were the FEM-FCT schemes. These schemes showed also the smallest errors in $L^2(H^1)$. Evaluating the results obtained in this example

leads basically to the same conclusions for each method as for the rotating body problem. It is an open question if the spurious oscillations behind the hump can be reduced by applying even better quadrature rules.

8. Summary

The summary contains a short discussion of the methods whose results are among the best ones.

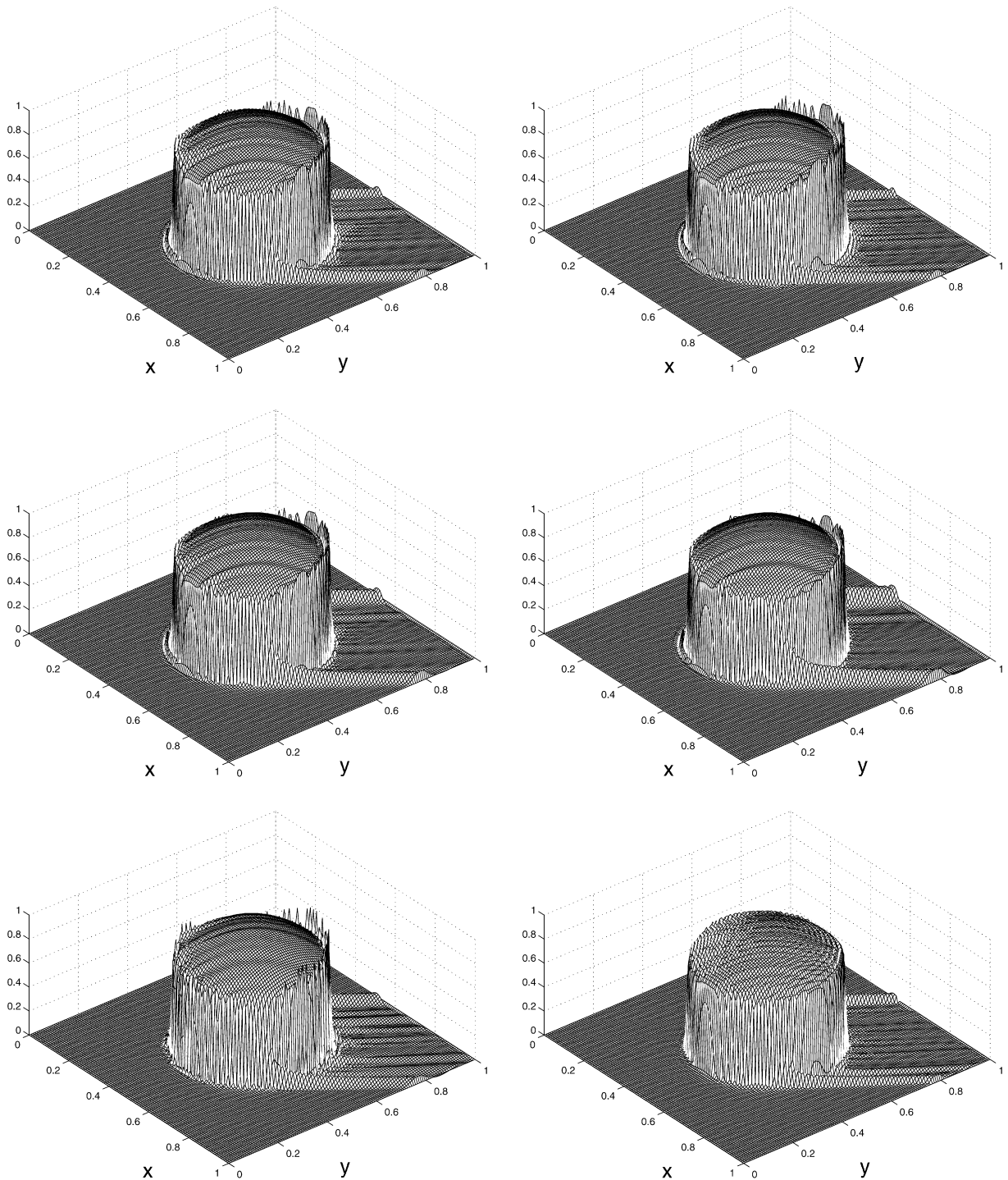


Fig. 16. Hump changing its height, the computed solution with P_1 at $t = 0.5$; the non-linear schemes $YZ\beta$ [54,2] anisotropic, KLR02 [42,34] with $C = 0.2$, $C = 0.4$, $C = 0.6$, BE05_2 [10,34] with $C = 1e - 1$ and FEM-FCT non-linear [45,44]; from top left to bottom right.

- JSW87: This is an easy linear extension of the SUPG method. In our studies, the spurious oscillations of the SUPG method were reduced considerably but not sufficiently. Note, the parameter of this method scales with the length of the time step and it has still to be studied which reductions of the oscillations can be achieved with different time steps. Altogether, this method seems to be not appropriate for the simulation of complex problems like chemical reactions in flow fields.

- KLR02: This was, in our opinion, the best SOLD method. Similar results could be obtained with C93 if the non-linear problems in this method could be solved. The difficulty in KLR02 is the presence of the user-chosen parameter. It is even hard to define a posteriori for the presented examples what is an optimal parameter, based on the criteria of spurious oscillations, smearing and computational overhead. Even more complicated will be the a priori choice of this parameter in complex applications.

- $YZ\beta$ aniso: This method gave in the considered examples similar results to KLRO2 with a parameter of $C \approx 0.4$.
- FEM-FCT schemes: These were clearly the best schemes. In Example 7.2 it is shown that these schemes may lead to some spurious oscillations. In particular, the linear FEM-FCT scheme shows a very good ratio of accuracy and efficiency. The smearing which is introduced by this scheme will be tolerable in many applications. This scheme has been identified to be a promising candidate to be used in the simulation of the chemical reactions in precipitation processes.

The evaluation of these methods has to be continued. In particular, examples with different boundary conditions than homogeneous Dirichlet boundary conditions and examples in three dimensions have to be investigated, see [40] for first results. In addition, the behavior of the methods with respect to changes in the length of the time step and the mesh size needs to be studied.

References

- [1] R.C. Almeida, R.S. Silva, A stable Petrov–Galerkin method for convection-dominated problems, *Comput. Methods Appl. Mech. Engrg.* 140 (1997) 291–304.
- [2] Y. Bazilevs, V.M. Calo, T.E. Tezduyar, T.J.R. Hughes, $YZ\beta$ discontinuity capturing for advection-dominated process with applications to arterial drug delivery, *Int. J. Numer. Methods Fluids* 54 (2007) 593–608.
- [3] R. Becker, M. Braack, A finite element pressure gradient stabilization for the Stokes equations based on local projections, *Calcolo* 28 (2001) 173–199.
- [4] P.B. Bochev, M.D. Gunzburger, J.N. Shadid, Stability of the SUPG finite element method for transient advection–diffusion problems, *Comput. Methods Appl. Mech. Engrg.* 193 (2004) 2301–2323.
- [5] M. Braack, E. Burman, Local projection stabilization for the Oseen problem and its interpretation as a variational multiscale method, *SIAM J. Numer. Anal.* 43 (2006) 2544–2566.
- [6] M. Braack, E. Burman, V. John, G. Lube, Stabilized finite element methods for the generalized Oseen problem, *Comput. Methods Appl. Mech. Engrg.* 196 (2007) 853–866.
- [7] A.N. Brooks, T.J.R. Hughes, Streamline upwind/Petrov–Galerkin formulations for convection dominated flows with particular emphasis on the incompressible Navier–Stokes equations, *Comput. Methods Appl. Mech. Engrg.* 32 (1982) 199–259.
- [8] E. Burman, A. Ern, Nonlinear diffusion and discrete maximum principle for stabilized Galerkin approximations of the convection–diffusion–reaction equation, *Comput. Methods Appl. Mech. Engrg.* 191 (2002) 3833–3855.
- [9] E. Burman, A. Ern, The discrete maximum principle for stabilized finite element methods, in: F. Brezzi, A. Buffa, S. Corsaro, A. Muri, Numerical mathematics and advanced applications, Proceedings of the Fourth European Conference (ENUMATH 2001), Springer, Italia, Milan, 2003, pp. 557–566.
- [10] E. Burman, A. Ern, Stabilized Galerkin approximation of convection–diffusion–reaction equations: discrete maximum principle and convergence, *Math. Comput.* 74 (2005) 1637–1652.
- [11] E. Burman, P. Hansbo, Edge stabilization for Galerkin approximations of convection–diffusion–reaction problems, *Comput. Methods Appl. Mech. Engrg.* 193 (2004) 1437–1453.
- [12] P.G. Ciarlet, The finite element method for elliptic problems, North-Holland Publishing Company, Amsterdam – New York – Oxford, 1978.
- [13] R. Codina, A discontinuity-capturing crosswind-dissipation for the finite element solution of the convection–diffusion equation, *Comput. Methods Appl. Mech. Engrg.* 110 (1993) 325–342.
- [14] R. Codina, Comparison of some finite element methods for solving the diffusion–convection–reaction equation, *Comput. Methods Appl. Mech. Engrg.* 156 (1998) 185–210.
- [15] R. Codina, On stabilized finite element methods for linear systems of convection–diffusion–reaction equations, *Comput. Methods Appl. Mech. Engrg.* 188 (2000) 61–82.
- [16] R. Codina, J. Blasco, Analysis of stabilized finite element approximation of the transient convection–diffusion–reaction equation using orthogonal subscales, *Comput. Vis. Sci.* 4 (2002) 167–174.
- [17] T.A. Davis, Algorithm 832: UMPACK V4.3—an unsymmetric-pattern multifrontal method, *ACM Trans. Math. Software* 30 (2004) 196–199.
- [18] E.G.D. do Carmo, G.B. Alvarez, A new stabilized finite element formulation for scalar convection–diffusion problems: the streamline and approximate upwind/Petrov–Galerkin method, *Comput. Methods Appl. Mech. Engrg.* 193 (2004) 1437–1453.
- [19] E.G.D. do Carmo, A.C. Galeão, Feedback Petrov–Galerkin methods for convection-dominated problems, *Comput. Methods Appl. Mech. Engrg.* 88 (1991) 1–16.
- [20] L.P. Franca, F. Valentin, On an improved unusual stabilized finite element method for the advective–reactive–diffusive equation, *Comput. Methods Appl. Mech. Engrg.* 190 (2000) 1785–1800.
- [21] A.C. Galeão, R.C. Almeida, S.M.C. Malta, A.F.D. Loula, Finite element analysis of convection dominated reaction–diffusion problems, *Appl. Numer. Math.* 48 (2004) 205–222.
- [22] A.C. Galeão, E.G.D. do Carmo, A consistent approximate upwind Petrov–Galerkin method for convection-dominated problems, *Comput. Methods Appl. Mech. Engrg.* 68 (1988) 83–95.
- [23] S. Ganesan, L. Tobiska, Stabilization by local projection. convection–diffusion and incompressible flow problems. Preprint 46, Otto-von-Guericke-Universität Magdeburg, Fakultät für Mathematik, 2007.
- [24] V. Gravemeier, W.A. Wall, A space-time formulation and improved spatial reconstruction for the “divide-and-conquer” multiscale method, *Comput. Methods Appl. Mech. Engrg.* 197 (2008) 678–692.
- [25] J.-L. Guermond, Stabilization of Galerkin approximations of transport equations by subgrid modeling, *M2AN* 33 (1999) 1293–1316.
- [26] G. Hauke, A simple subgrid scale stabilized method for the advection–diffusion–reaction equation, *Comput. Methods Appl. Mech. Engrg.* 191 (2002) 2925–2947.
- [27] G. Hauke, M.H. Doweidar, Fourier analysis of semi-discrete and space-time stabilized methods for the advective–diffusive–reactive equation: II. SGS, *Comput. Methods Appl. Mech. Engrg.* 194 (2005) 691–725.
- [28] T.J. Hughes, L. Mazzei, K.E. Jansen, Large eddy simulation and the variational multiscale method, *Comput. Visual. Sci.* 3 (2000) 47–59.
- [29] T.J.R. Hughes, Multiscale phenomena: Green’s functions, the Dirichlet-to-Neumann formulation, subgrid-scale models, bubbles and the origin of stabilized methods, *Comput. Methods Appl. Mech. Engrg.* 127 (1995) 387–401.
- [30] T.J.R. Hughes, A.N. Brooks, A multidimensional upwind scheme with no crosswind diffusion, in: T.J.R. Hughes (Ed.), *Finite Element Methods for Convection Dominated Flows*, AMD, vol. 34, ASME, New York, 1979, pp. 19–35.
- [31] V. John, On large eddy simulation and variational multiscale methods in the numerical simulation of turbulent incompressible flows, *Appl. Math.* 51 (2006) 321–353.
- [32] V. John, S. Kaya, A finite element variational multiscale method for the Navier–Stokes equations, *SIAM J. Sci. Comput.* 26 (2005) 1485–1503.
- [33] V. John, S. Kaya, W. Layton, A two-level variational multiscale method for convection-dominated convection–diffusion equations, *Comput. Meth. Appl. Math. Engrg.* 195 (2006) 4594–4603.
- [34] V. John, P. Knobloch, A comparison of spurious oscillations at layers diminishing (sold) methods for convection–diffusion equations: part I – a review, *Comput. Methods Appl. Mech. Engrg.* 196 (2007) 2197–2215.
- [35] V. John, P. Knobloch, On the performance of SOLD methods for convection–diffusion problems with interior layers, *Int. J. Comput. Sci. Math.* 1 (2007) 245–258.
- [36] V. John, P. Knobloch, A comparison of spurious oscillations at layers diminishing (sold) methods for convection–diffusion equations: part II – analysis for P_1 and Q_1 finite elements, *Comput. Methods Appl. Mech. Engrg.* 197 (2008) 1997–2014.
- [37] V. John, G. Matthies, MoonMMD – a program package based on mapped finite element methods, *Comput. Visual. Sci.* 6 (2004) 163–170.
- [38] V. John, J.M. Maubach, L. Tobiska, Nonconforming streamline–diffusion–finite-element-methods for convection–diffusion problems, *Numer. Math.* 78 (1997) 165–188.
- [39] V. John, M. Roland, T. Mitkova, K. Sundmacher, L. Tobiska, A. Voigt, Simulations of population balance systems with one internal coordinate using finite element methods, *Chem. Engrg. Sci.*, in press.
- [40] V. John, E. Schmeier, On finite element methods for 3d time-dependent convection–diffusion–reaction equations with small diffusion. Preprint 219, Universität des Saarlandes, Fachrichtung 6.1 – Mathematik, 2008. submitted to the Proceedings of the Conference BAIL 2008, Limerick.
- [41] C. Johnson, A.H. Schatz, L.B. Wahlbin, Crosswind smear and pointwise errors in streamline diffusion finite element methods, *Math. Comput.* 49 (1987) 25–38.
- [42] T. Knopp, G. Lube, G. Rapin, Stabilized finite element methods with shock capturing for advection–diffusion problems, *Comput. Methods Appl. Mech. Engrg.* 191 (2002) 2997–3013.
- [43] D. Kuzmin, Explicit and implicit FEM-FCT algorithms with flux linearization, *Ergebnisberichte Angew. Math.* 358, University of Dortmund, 2008.
- [44] D. Kuzmin, M. Möller, Algebraic flux correction I. Scalar conservation laws, in: R. Löhner, M. Kuzmin, S. Turek (Eds.), *Flux-Corrected Transport: Principles, Algorithms and Applications*, Springer, 2005, pp. 155–206.
- [45] D. Kuzmin, M. Möller, S. Turek, High-resolution FEM-FCT schemes for multidimensional conservation laws, *Comput. Methods Appl. Mech. Engrg.* 193 (2004) 4915–4946.
- [46] D. Kuzmin, S. Turek, Flux correction tools for finite elements, *J. Comput. Phys.* 175 (2002) 525–558.
- [47] R.J. LeVeque, High-resolution conservative algorithms for advection in incompressible flow, *SIAM J. Numer. Anal.* 33 (1996) 627–665.
- [48] R. Löhner, K. Morgan, J. Peraire, M. Vahdati, Finite element flux-corrected transport (FEM-FCT) for the Euler and Navier–Stokes equations, *Int. J. Numer. Methods Fluids* 7 (1987) 1093–1109.
- [49] G. Lube, G. Rapin, Residual-based stabilized higher-order FEM for advection-dominated problems, *Comput. Methods Appl. Mech. Engrg.* 195 (2006) 4124–4138.
- [50] G. Matthies, P. Skrzypacz, L. Tobiska, Stabilisation of local projection type applied to convection–diffusion problems with mixed boundary conditions.

- Preprint 44, Otto-von-Guericke-Universität Magdeburg, Fakultät für Mathematik, 2007.
- [51] G. Matthies, P. Skrzypacz, L. Tobiska, A unified convergence analysis for local projection stabilisations applied to the Oseen problem, *M2AN* 41 (2007) 713–742.
- [52] H.-G. Roos, M. Stynes, L. Tobiska, *Numerical Methods for Singularly Perturbed Differential Equations*, Springer, 1996.
- [53] M. Stynes, L. Tobiska, Necessary L^2 -uniform convergence conditions for difference schemes for two-dimensional convection–diffusion problems, *Comput. Math. Appl.* 29 (1995) 45–53.
- [54] T.E. Tezduyar, Finite element methods for fluid dynamics with moving boundaries and interfaces, in: E. Stein, R. De Borst, T.J.R. Hughes (Eds.), *Encyclopedia of Computational Mechanics, Fluids*, vol. 3, Wiley, New York, 2004. chapter 17.
- [55] T.E. Tezduyar, Y.J. Park, Discontinuity-capturing finite element formulations for nonlinear convection–diffusion–reaction equations, *Comput. Methods Appl. Mech. Engrg.* 59 (1986) 307–325.
- [56] S.T. Zalesak, Fully multi-dimensional flux corrected transport algorithms for fluid flow, *J. Comput. Phys.* 31 (1979) 335–362.